ESC European Society of Cardiology

Cardiovascular Research (2024) **120**, 403–416
https://doi.org/10.1093/cvr/cvae011

Endothelium-specific SIRT7 targeting ameliorates pulmonary hypertension through Krüpple-like factor 4 deacetylation

Jin Zhang[1,2], Chenzhong Xu[1,2], Xiaolong Tang[2], Shimin Sun[2], Siqi Liu[2], Langmei Yang[2], Yuqin Chen[3], Qifeng Yang[3], Tong-You Wade Wei[4], Xiaojing Wu[5], Jian Wang[3,6], Chen Wang[7], Xiaosong Yan[8], Lei Yang[9], Yanqin Niu[9], Deming Gou[9]*, John Y.-J. Shyy[4]*, and Baohua Liu[2]*

[1]Guangdong Key Laboratory for Biomedical Measurements and Ultrasound Imaging, National-Regional Key Technology Engineering Laboratory for Medical Ultrasound, Marshall Laboratory of Biomedical Engineering, School of Biomedical Engineering, Shenzhen University Medical School, Shenzhen 518060, China; [2]Shenzhen Key Laboratory for Systemic Aging and Intervention (SKL-SAI), International Cancer Center, School of Basic Medical Sciences, Shenzhen University Medical School, 1066 Xueyuan Blvd, Nanshan District, Shenzhen 518055, China; [3]State Key Laboratory of Respiratory Diseases, National Center for Respiratory Medicine, Guangdong Key Laboratory of Vascular Diseases, National Clinical Research Center for Respiratory Diseases, Guangzhou Institute of Respiratory Health, the First Affiliated Hospital of Guangzhou Medical University, Guangzhou Medical University, Guangzhou, Guangdong 510120, China; [4]Division of Cardiology, Department of Medicine, University of California, San Diego 9500 Gilman Dr, La Jolla, CA 92023, USA; [5]Cardiovascular Department of Shenzhen University General Hospital, Shenzhen 518055, China; [6]Guangzhou Laboratory, Guangzhou International Bio Island, Guangzhou, Guangdong 510005, China; [7]Department of Cardiology, First Affiliated Hospital of Xi'an Jiaotong University, Xi'an, Shaanxi 710061, China; [8]Department of Pathology, The Affiliated Children's Hospital of Xi'an Jiaotong University, Xi'an, Shaanxi 710003, China; and [9]Shenzhen Key Laboratory of Microbial Genetic Engineering, Guangdong Provincial Key Laboratory of Regional Immunity and Diseases, Vascular Disease Research Center, College of Life Sciences and Oceanography, Shenzhen University, 1066 Xueyuan Blvd, Nanshan District, Shenzhen, 518060, China

Received 9 May 2023; revised 11 November 2023; accepted 29 November 2023; online publish-ahead-of-print 10 January 2024

Time of primary review: 33 days

Aims

Pulmonary hypertension (PH) is a pulmonary vascular disease characterized by a high mortality rate. Pulmonary arterial endothelium cells (PAECs) serve as a primary sensor of various environmental cues, such as shear stress and hypoxia, but PAEC dysfunction may trigger vascular remodelling during the onset of PH. This study aimed to illustrate the role of Sirtuin 7 (SIRT7) in endothelial dysfunction during PH and explore the potential therapeutic strategy for PH.

Methods and results

SIRT7 levels were measured in human and murine experimental PH samples. Bioinformatic analysis, immunoprecipitation, and deacetylation assay were used to identify the association between SIRT7 and Krüpple-like factor 4 (KLF4), a key transcription factor essential for endothelial cell (EC) homeostasis. Sugen5416 + hypoxia (SuHx)-induced PH mouse models and cell cultures were used for the study of the therapeutic effect of SIRT7 for PH. SIRT7 level was significantly reduced in lung tissues and PAECs from PH patients and the SuHx-induced PH mouse model as compared with healthy controls. Pulmonary endothelium-specific depletion of *Sirt7* increased right ventricular systolic pressure and exacerbated right ventricular hypertrophy in the SuHx-induced PH model. At the molecular level, we identified KLF4 as a downstream target of SIRT7, which deacetylated KLF4 at K228 and inhibited the ubiquitination-proteasome degradation. Thus, the SIRT7/KLF4 axis maintained PAEC homeostasis by regulating proliferation, migration, and tube formation. PAEC dysfunction was reversed by adeno-associated virus type 1 vector-mediated endothelial overexpression of *Sirt7* or supplementation with nicotinamide adenine dinucleotide $(NAD)^+$ intermediate nicotinamide riboside which activated Sirt7; both approaches successfully reversed PH phenotypes.

Conclusion

The SIRT7/KLF4 axis ensures PAEC homeostasis, and pulmonary endothelium-specific SIRT7 targeting might constitute a PH therapeutic strategy.

* Corresponding author. Tel: +86 755 2691 5563, fax: 86755-86694609, E-mail: ppliew@szu.edu.cn (B.L.); Tel: +86 158 6131 3428, E-mail: jshyy@health.ucsd.edu (J.Y.-J.S.); Tel: +86 139 2458 4169, E-mail: dmgou@szu.edu.cn (D.G.).

Graphical Abstract

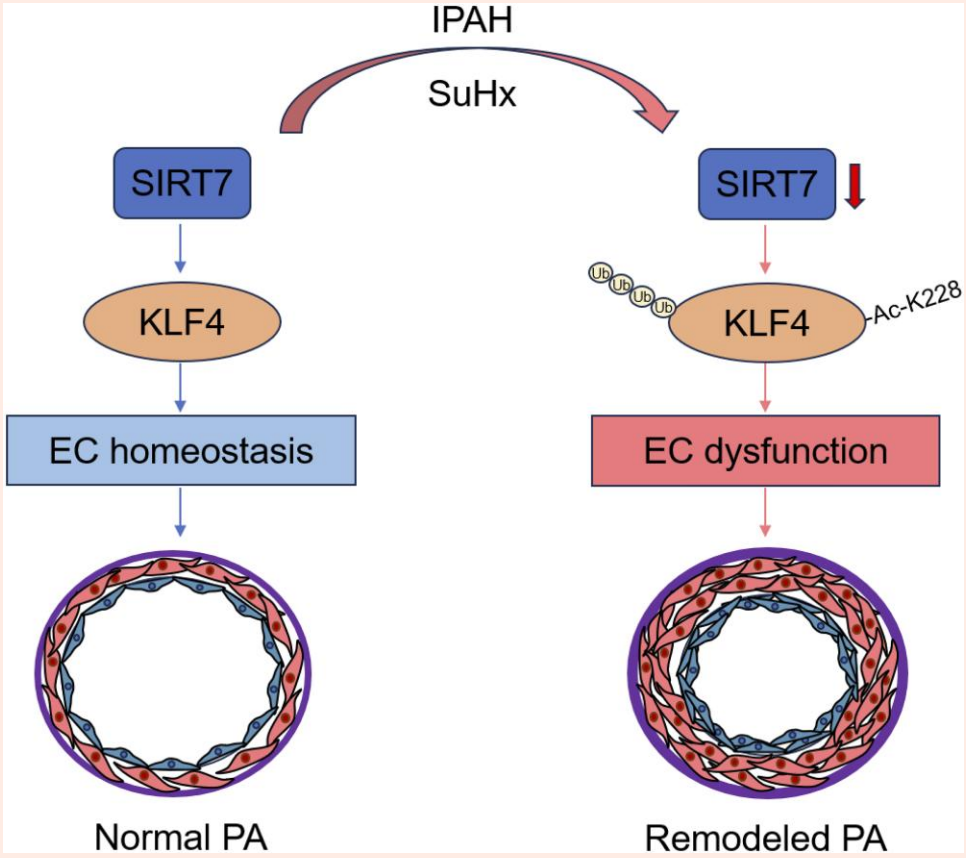

In normal pulmonary artery endothelial cells (ECs), SIRT7 deacetylates KLF4 at K228 to maintain its protein stability and promotes endothelial homeostasis and pulmonary vascular function. During pulmonary hypertension (PH) pathogenesis, SIRT7 was reduced, resulting in increased acetylation of KLF4 and promoting its ubiquitination and degradation in pulmonary ECs. The ultimate endothelial dysfunction contributes to vascular remodelling and accelerated PH.

Keywords SIRT7 • endothelial cells • pulmonary hypertension • KLF4

1. Introduction

Pulmonary hypertension (PH) is characterized by increased pulmonary arterial pressure (>25 mmHg) with ensuing right ventricular hypertrophy.[1] The involvement of endothelial dysfunction in pulmonary arterial hypertension (PAH) has gained attention recently.[2] Pulmonary ECs are directly and continuously exposed to a variety of exogenous stimuli, including shear stress, hypoxia, infection, and inflammatory factors. Ultimately, this leads to endothelial dysfunction, which initiates vascular remodelling leading to the pathogenesis of PAH.[3,4]

Vascular endothelial dysfunction is common during aging, which is usually caused by replicative stress, telomere shortening and inflammation and is characterized by the abnormal secretion of vasoconstrictors and inflammatory cytokines.[5] Consistently, PH is prevalent in older patients (50–65 years old).[6] Pulmonary ECs are sensitive to senescence, as evidenced by elevated expression of *CDKN2A*/p16^{INK4A} and increased senescence-associated β-galactosidase activity in PH patients. Senescent ECs develop a senescence-associated secretory phenotype (SASP), including interleukins [e.g. interleukin-1β (IL-1β), IL-6], cytokines [e.g. monocytic chemotactic protein 1 (MCP-1)], and growth factors, which is consistent with the pro-inflammatory transition of ECs during PH pathogenesis.[3] Senescent pulmonary ECs produce less nitric oxide (NO) and prostacyclin, with suppressed angiogenic capacity. This likely contributes to vascular remodelling, vasoconstriction, and vascular stiffness during PH development.[7] Senolytic therapy with ABT-263 restored EC function in PH.[8] Thus, the mechanisms underlying pulmonary endothelial dysfunction that links senescence to PH warrant in-depth investigation.

Sirtuins are NAD^+-dependent deacylases that are closely associated with health and longevity in humans and animals.[9] During aging, NAD^+ level is reduced, and sirtuins expression and function are attenuated.[10] *Sirt1* deficiency in mice exacerbates PH by altering mitochondrial function, which promotes the proliferation of pulmonary arterial smooth muscle cells (PASMCs).[11] The level of SIRT3, mainly localized in mitochondria, is reduced in PASMCs in PAH patients and PH rat models. *Sirt3*-deficient mice develop spontaneous PH with increased vascular endothelial growth factor a (VEGFA) and hypoxia-inducible factor 1α (HIF-1α) expression in PASMCs.[12] SIRT7 is unique among the sirtuin family in that it is localized in the nucleolus, where it helps maintain chromatin stability, circadian rhythmicity, metabolism, and cell survival via the deacylation of histones and non-histones.[13–17] SIRT7 is known to confer protective effects on endothelium.[18] SIRT7 level is decreased in both patients and rodent models with pulmonary fibrosis, with increased expression of collagen and α-smooth muscle actin (α-SMA).[19] Depletion of *Sirt7* in mice exacerbates lipopolysaccharide-induced endothelial-to-mesenchymal transition and permeability of pulmonary ECs during acute lung injury.[20] We recently found that SIRT7 protects endothelial function in a model of premature aging and, therefore, hypothesized that SIRT7 plays a pivotal role in endothelium in the context of PH.[18] Krüpple-like factor 4 (KLF4) is a critical

transcription factor for endothelial homeostasis.[21] KLF4 expression is reduced in lung tissues of patients with idiopathic PAH (IPAH), and *Klf4* deficiency in ECs promotes PH development in rodent models.[22] In the present study, we used genetically modified models and adeno-associated virus (AAV) vector-mediated gene delivery to show the beneficial role of SIRT7 in mitigating PH via deacetylating KLF4.

2. Methods

2.1 Human lung samples

Human lung specimens were from explanted lungs from healthy individuals or patients with IPAH undergoing lung transplantation at the First Affiliated Hospital of Guangzhou Medical University; written informed consent was obtained from all participants. All patients were given a diagnosis based on the criteria for PAH according to the European Society of Cardiology/European Respiratory Society guidelines for the diagnosis. Pulmonary arterial endothelium cells (PAECs) of IPAH patients and control individuals were obtained from the PH Breakthrough Initiative at UPenn. The study was approved by the institutional review board of the First Affiliated Hospital of Guangzhou Medical University and the University of California, San Diego. The investigation conformed to the principles outlined in the Declaration of Helsinki. Demographic and clinical data for controls and IPAH patients are in Supplementary material online, *Table S1*.

2.2 Animal models

Sirt7 knockout (KO), *Sirt7*$^{f/f}$, and Tet-on *Sirt7*-transgenic (*Sirt7*-Tg) mice were created and bred as previously described.[14,23] *Sirt7* transgene expression was induced by oral application of doxycycline (Dox) diluted in drinking water (1 mg/mL) at 4 weeks old for at least 7 days. *Sirt7*$^{f/f}$ mice were crossed with Cdh5-cre/estrogen receptor (ERT) mice to generate *Sirt7*$^{f/f}$; Cdh5-cre/ERT mice. Six-week-old *Sirt7*$^{f/f}$; Cdh5-cre/ERT mice were intraperitoneally injected with tamoxifen (20 mg/mL and 75 mg/kg body weight) daily for 5 days to obtain endothelium-specific *Sirt7*-KO mice. *Sirt7* deletion was verified by detecting Sirt7 protein levels in lung ECs. All animal studies were approved by the Institutional Animal Ethics Committee of Shenzhen University (Shenzhen, China) and were in accordance with the NIH Guide for the Care and Use of Laboratory Animals.

2.3 Cell cultures

Human PAECs were purchased from ScienCell Research Laboratories (Carlsbad, CA, USA) and cultured with endothelial culture medium (ECM; ScienCell Research Laboratories). Human embryonic kidney 293T (HEK293T) cells were obtained from ATCC (Manassas, VA, USA) and cultured using dulbecco's modified eagle medium (DMEM) (Corning, Inc., Corning, NY, USA). PAECs in passages 4–7 were used for all cell culture experiments. Murine lung ECs were isolated as described.[24] All cells were cultured at 37 °C with 5% CO_2 and 95% relative humidity.

2.4 Plasmids and constructs

Human HA-HIF-2α, FLAG-SIRT7, and HA-KLF4 constructs were generated by using a PCR-dependent sequence cloned into pcDNA3.1 vectors. Truncated KLF4 plasmids were constructed by PCR-based deletion, with HA-KLF4 as a template. KLF4 lysine mutants were generated by using a QuikChange Site-Directed Mutagenesis kit (Stratagene California, San Diego, CA, USA). All constructs were verified by DNA sequencing (Ruibiotech, Guangzhou, China). The siRNA sequence against *HIF2A* and *SIRT7* was 5′-GCAAAUGUACCCAAUGAUATT-3′ and 5′-CUCACC GUAUUUCU ACUACUA-3′ and was synthesized by GenePharma Co. (Suzhou, China). Plasmids and siRNAs were transfected with Lipofecatmine3000 (Thermo Fisher Scientific, Waltham, MA, USA) according to the manufacturer's protocol. Recombinant adeno-associated virus 1 (rAAV1) overexpressing sh*Sirt7* and recombinant AAV serotype 1 cassette with *Cre* or *Sirt7* gene expression driven by a synthetic *ICAM2* promoter [rAAV1-*ICAM2-Cre* and rAAV1-*ICAM2-Sirt7* (IS7O)] were created by Weizhen Bioengineering Technology (Anhui, China). The sh*Sirt7* sequence was 5′-TGCATCCCTAACAGAGAGTAT-3′. Lentivirus vectors overexpressing *SIRT7* were constructed by cloning *SIRT7* coding DNA sequence (CDS) into pLEX vectors and then transfecting these into HEK293T cells, along with VSVG and pCMV-R8.2 for packaging. After transfection for 48 h, cell supernatants were collected and filtered through 0.45 μm membranes (Millipore; Merck KGaA, Darmstadt, Germany) before being used to infect cells.

2.5 PH rodent models and haemodynamic measurement

Mice were kept on a 12-h light/dark cycle at 22 °C and fed *ad libitum* with a standard chow diet. Male C57BL/6 mice (8–12 weeks old) were subjected to inhalation delivery of rAAV1-sh*Sirt7* (shS7), rAAV1-*ICAM2-Cre* (ICre), rAAV1-IS7O, or control viral particles at 10^{11} Plaque Forming Unit (PFU) concentration twice, with one administration per week. Two weeks after delivery, mice were subcutaneously injected with 20 mg/kg Sugen5416 or dimethylsulfoxide (DMSO) and then exposed to hypoxia (10% oxygen) once a week for 3 weeks. Male *Sirt7*$^{f/f}$ mice (8–12 weeks old) were likewise challenged with inhalation of ICre or IS7O once a week for 2 weeks, then exposed to Sugen5416 (20 mg/kg) followed by hypoxia to induce PH. For NAM riboside (NR) treatment, mice were supplemented with NR orally at 400 mg/kg/day for 1 week. Mice were anaesthetized via 1% isoflurane inhalation for measuring haemodynamics. Right ventricular systolic pressure (RVSP) was measured using standard protocols. Before the isolation of tissues, mice were euthanized with 4% isoflurane. The Fulton index (ratio of right ventricle weight to left ventricle plus interventricular septum weight, RV/[LV + S]), was used to assess right ventricular (RV) hypertrophy. Pulmonary artery thickness (~20 μm diameter, $n = 20$ for each animal) was measured using a picture scale plate. For pulmonary angiography, mice were anaesthetised by pentobarbital sodium (120 mg/kg), and then, phosphate buffered saline (PBS) was injected into the right ventricle to wash out blood in the pulmonary arteries. Next, Microfil polymers were injected into the pulmonary artery. Lungs were dehydrated using ethanol, followed by methyl salicylate culture. ImageJ® was used to quantify the length of vascular branches, number of branches, and branch junctions of lung tissues.

2.6 Immunofluorescence

Formaldehyde-fixed, paraffin-embedded human lung tissue sections were deparaffined and rehydrated. Sections were blocked with 2.5% Bovine Serum Albumin (BSA) and incubated with the primary anti-SIRT7 (Santa Cruz Biotechnology, Dallas, TX, USA, cat. no. sc-365344, 1:100 dilution) and anti-CD31 (Abcam, Cambridge, UK, cat.no. ab222783, 1:200 dilution) overnight and then stained with an Alexa Fluo 488-conjugated goat anti-mouse and Cy5-conjugated goat anti-rabbit secondary antibody (Servicebio, Wuhan, China,1:400 dilution) for 1 h. Slides were visualized by laser scanning confocal microscopy (KF-PRO-005, KFBIO, Yuyao, China).

2.7 Proliferation and migration assays

PAEC proliferation was measured by 5-ethynyl-2′-deoxyuridine (EdU) incorporation with the BeyoClick EdU Cell Proliferation Kit with Alexa Fluor 594 (Beyotime Institute of Biotechnology, Shanghai, China), according to the manufacturer's instructions. PAEC migration was assessed by wound healing assay. In brief, PAECs were plated in six-well plates. Cells were cultured in 0.1% or 5% Foetal Bovine Serum (FBS) for 24 h. Wounds were generated by moving a sterile 200-μL pipette tip through the cells when they reached about 90% confluence. The wounds were photographed randomly 4 h later by Zeiss Axio Ver.A1 Light Microscopy (Carl Zeiss Microscopy GmbH, Jena, Germany), and the widths of wounded areas were measured.

2.8 Tube formation assay

Growth-factor reduced Matrigel (Corning) was dissolved and used to coat a 24-well plate (200 μL per well). Then, human PAECs were seeded onto the Matrigel at 1×10^6 cells/well. Zeiss Axio Ver.A1 Light Microscopy was

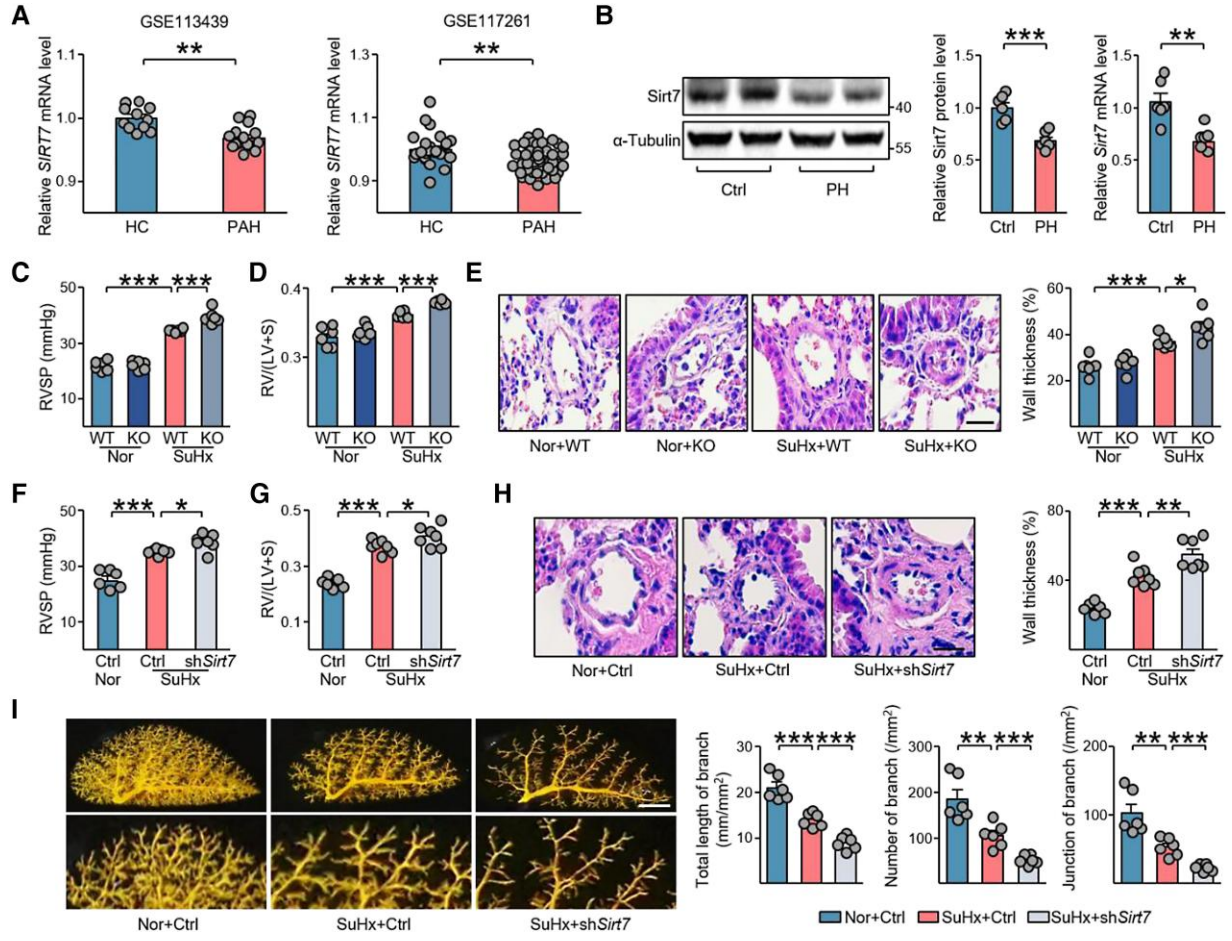

Figure 1 SIRT7 deficiency exacerbates PH. (*A*) Relative *SIRT7* mRNA levels in lung tissues from PAH patients ($n = 15$) compared to HC ($n = 11$) (GSE113439) and in lung tissues from PAH patients ($n = 58$) compared with HC ($n = 25$) obtained from GSE117261. (*B*) Sirt7 protein and mRNA levels in SuHx-induced PH mice (PH, $n = 6$) and control mice (Ctrl, $n = 6$) lung tissues measured by western blotting and qPCR analysis, respectively. (*C–E*) Eight-week-old *Sirt7*-KO mice ($n = 6$) and their WT littermates ($n = 6$) were exposed to normoxia (Nor) or SuHx for 4 weeks. RVSP (*C*) and Fulton Index (*D*) were measured. (*E*) Pulmonary arterial wall thickness of Nor + WT, Nor + KO, SuHx + WT and SuHx + KO mice, as shown by H&E staining. Scale bar = 20 μm. (*F–I*) Eight-week-old C57BL/6 mice inhaled with AAV1-vehicle (Ctrl) or rAAV1-sh*Sirt7* (sh*Sirt7*). Two weeks later, they were exposed to normoxia or SuHx for 4 weeks. RVSP (*F*) and Fulton Index (RV/[LV + S], *G*) were measured. (*H*) H&E staining of pulmonary arteries and quantified data showing the pulmonary arterial wall thickness of Nor + Ctrl ($n = 6$), SuHx + Ctrl ($n = 7$), and SuHx + sh*Sirt7* ($n = 7$) mice. Scale bar = 20 μm. (*I*) Angiogram of left lungs from mice of indicated groups. Scale bar = 1 mm. Quantified data show the total length of branches, number of branches, and number of junctions of the left lungs, $n = 6$ for each group. Data are means ± SEM. Data were analysed by (*A*) Mann–Whitney *U* test, two-tailed Student *t*-test (*B*), and (*C–E*) two-way ANOVA with Holm-Šídák's post-hoc test, and (*F–I*) Kruskal–Wallis test with Dunn post-hoc test for multiple groups. *$P < 0.05$, **$P < 0.01$, ***$P < 0.001$ with comparisons indicated by lines.

used to image cell tube formation at 6 h after seeding. ImageJ was used to measure the resulting tube and branch number.

2.9 Transcription factor binding motif analysis

Information concerning mRNAs of interest was obtained by using the UCSC Genome Browser (https://genome.ucsc.edu/, version GRCh37). The genomic sequences of promoter regions (−1000 bp to +500 bp to transcription start site) were obtained and adjusted to Multiple Em for Motif Elicitation (MEME) (http://meme-suite.org/) for motif analysis.[25]

2.10 Co-immunoprecipitation assays

Co-immunoprecipitation (Co-IP) assays were performed according to previously established protocols. In brief, total protein content was extracted with IP lysis buffer [150 mM NaCl, 25 mM Tris–HCl (pH 7.9), 5 mM $MgCl_2$, 10% glycerol, 0.2 mM Ethylene Diamine Tetraacetic Acid (EDTA), 0.1% Tergitol-type NP-40] containing protease inhibitor (Roche Holding AG, Basel, Switzerland). Appropriate antibodies and protein tag-fused beads (Sigma-Aldrich; Merck KGaA, Darmstadt, Germany) were used for the pull-down experiment. After washing, pull-down proteins were extracted from the beads and used for further Western blotting analysis.

2.11 Glutathione s-transferase pull-down assay

FLAG-KLF4 and glutathione s-transferase (GST)-SIRT7 were purified from BL21 *E. coli* GST or GST-SIRT7 protein (1 μg) was immobilized on glutathione-Sepharose 4B and then incubated with FLAG-KLF4 in GST

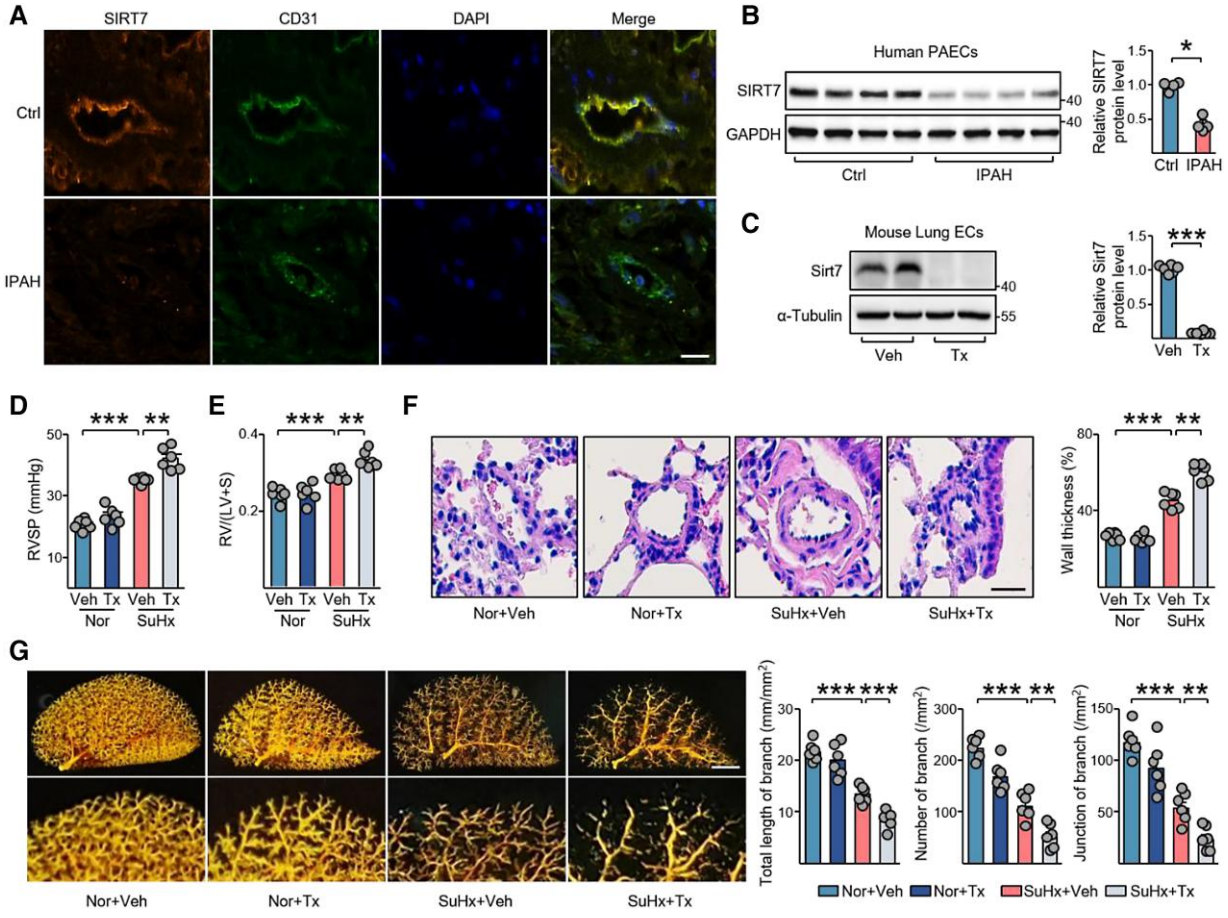

Figure 2 Endothelial-specific loss of *Sirt7* aggravates PH. (*A*) Immunofluorescence images of SIRT7 co-stained with CD31 in pulmonary arteries from lung tissues of IPAH patients ($n = 4$) and control individuals ($n = 2$). Scale bar = 20 μm. (*B*) Protein levels of SIRT7 in human PAECs isolated from IPAH patients ($n = 4$) and control individuals (Ctrl, $n = 4$). (*C*) Western blotting analysis of Sirt7 protein expression in lung ECs isolated from *Sirt7*$^{f/f}$; Cdh5-Cre^{ERT} mice intraperitoneally injected with TX (Tx, $n = 6$) or vehicle (Veh, $n = 6$). (*D–G*) Four-week-old *Sirt7*$^{f/f}$; Cdh5-Cre^{ERT} mice were intraperitoneally injected with Tx or vehicle (Veh). Four weeks later, mice were exposed to normoxia (Nor) or SuHx for 4 weeks. RVSP (*D*) and Fulton Index (*E*) were measured. Vascularization of mice in various groups were shown by H&E staining (*F*) and angiography (*G*) of lung tissues. Scale bar = 20 μm (*F*) and 1 mm (*G*), respectively. Data are means ± SEM, and were analysed using Mann–Whitney *U* test (*B*), two-tailed Student *t*-test (*C*), and two-way ANOVA with Holm-Šídák's post-hoc test for multiple groups (*D–G*). *$P < 0.05$, **$P < 0.01$, ***$P < 0.001$ with comparisons indicated by lines ($n = 6$ mice per group).

binding buffer (20 mM Tris–HCl, pH 7.4, 0.1 mM EDTA, 150 mM NaCl, 0.2% NP-40, protease inhibitors cocktail) for 2 h at 4 °C. The beads were washed three times with GST wash buffer (20 mM Tris–HCl, pH 7.4, 0.1 mM EDTA, 250 mM NaCl, and 0.2% NP-40) at 4 °C. Bead-bound proteins were then analysed with SDS–PAGE and western blotting.

2.12 *In vitro* deacetylation assays

FLAG-KLF4 was overexpressed in HEK293T cells and purified using Anti-FLAG M2 Affinity Gel (Sigma-Aldrich; Merck KGaA). Purified FLAG-KLF4 (2 μg) was incubated with 1 μg GST-SIRT7 in deacetylation buffer (25 mM Tris–HCl, pH 8.0, 1 mM $MgCl_2$, 137 mM NaCl, 2.7 mM KCl, 1 mM NAD^+ and protease inhibitor cocktail) for 1 h at 30 °C. KLF4 acetylation levels were measured by western blotting with antibodies targeting acetyl-lysine (PTM Biolabs, Hangzhou, China).

2.13 RNA extraction and real-time-qPCR

Total RNA was isolated from cells or lung tissues with TRIzol (Invitrogen; Thermo Fisher Scientific). The extracted RNA was reverse transcribed into complementary DNA by using a PrimeScript RT Master kit (Takara Bio, Shiga, Japan), and the cDNA was used as a real-time-qPCR template. SYBR Mix (Takara Bio) was used for qPCR according to the manufacturer's protocol. Primer sequences are presented in Supplementary material online, *Table S2*.

2.14 Western blotting analysis

Total protein content was isolated from cells by radioimmunoprecipitation assay (RIPA) lysis (Solarbio Science & Technology, Beijing, China), resolved by SDS–PAGE, and transferred onto polyvinylidene fluoride (PVDF) membranes (Millipore; Merck KGaA, Darmstadt, Germany). The membranes were labelled with primary antibodies at 4 °C overnight, followed by secondary antibodies at room temperature for 1 h, and visualized by using enhanced chemiluminescence (ECL) buffer (Thermo Fisher Scientific). ImageJ was used to analyse protein levels for each sample. The antibodies used were SIRT7 (Santa Cruz Biotechnology, cat. no. sc-365344, 1:3000 dilution), KLF4 (Cell Signaling Technology, Danvers, MA, USA, cat. no. 4038S, 1:1000 dilution), HIF-2α (Santa Cruz Biotechnology, cat. No. sc-13596, 1:1000 dilution), endothelial NO synthase (eNOS) (Cell Signaling Technology, cat. no. 9572, 1:1000 dilution),

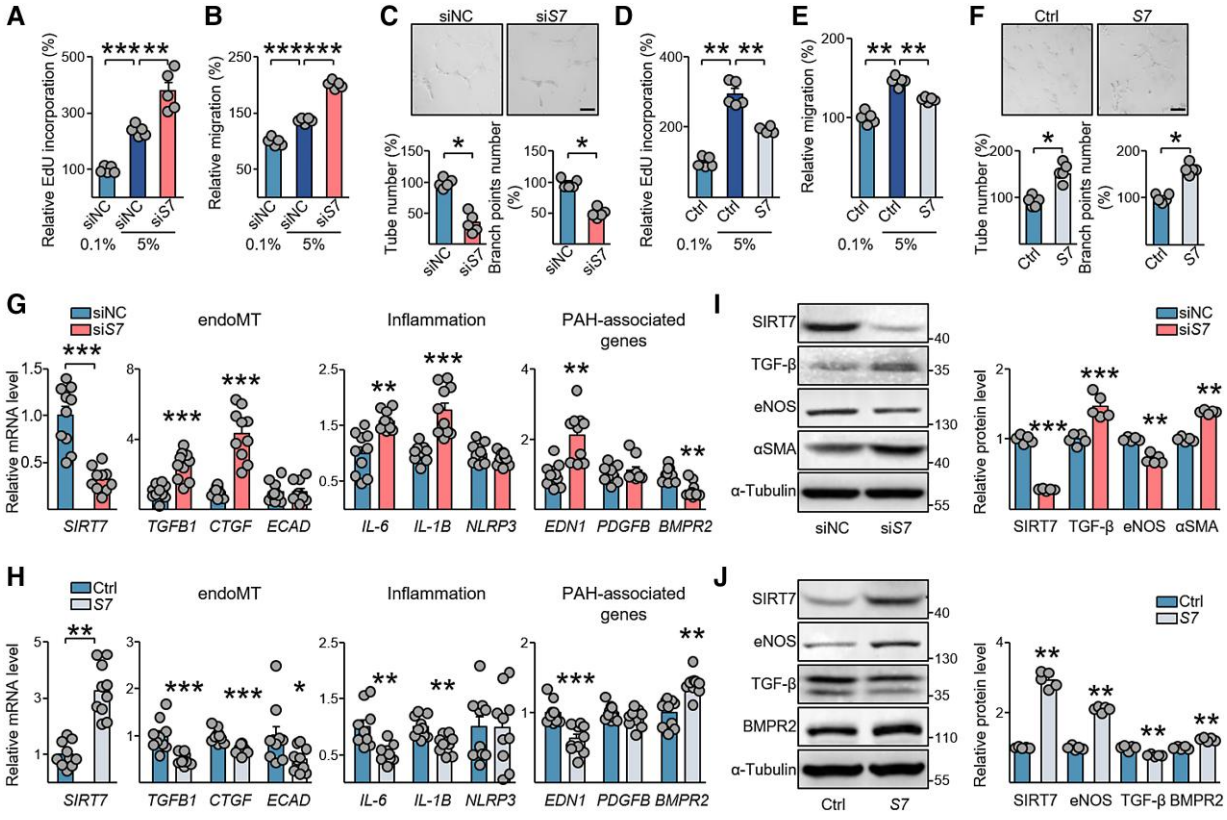

Figure 3 SIRT7 maintains PAEC function. (*A–F*) PAECs transfected with siRNA against *SIRT7* (si*S7*) or negative control (siNC), or infected with lentivirus-*SIRT7* (*S7*) or control virus (Ctrl), were cultured in either 0.1% or 5% FBS for 48 h. Proliferation (*A*, *D*) and migration (*B*, *E*) were measured by EdU and wound healing assays, respectively. Tube formation analysis using PAECs transfected with siNC or si*SIRT7*, or infected with Ctrl and lentivirus-*SIRT7* for 48 h. (*C*, *F*) Quantified data shows the number of tubes and branch points for each group. Scale bar = 20 μm. (*G*, *I*) qPCR measurement of *SIRT7*, *TGFB1*, *CTGF*, *cadherin 1 (ECAD)*, *IL-6*, *IL-1B*, *NLRP3*, *EDN1*, *platelet derived growth factor subunit B (PDGFB)* and *BMPR2* in PAECs transfected with siNC or si*SIRT7*, or infected with indicated lentivirus for 48 h. (*H*) Western blotting analysis of protein levels of SIRT7, TGF-β, eNOS, and α-SMA in PAECs transfected with siNC or si*S7* for 48 h, and (*J*) protein levels of SIRT7, eNOS TGF-β, and BMPR2 in PAECs with or without SIRT7 overexpression for 48 h. Data are means ± SEM from 5 or 10 independent experiments, and were analysed by Kruskal–Wallis test with Dunn post-hoc test (*A*, *B*, *D*, and *E*) and Student *t*-test or Mann–Whitney *U* test (*C*, *F*, *G–J*), $*P < 0.05$, $**P < 0.01$, $***P < 0.001$ with comparisons indicated by lines.

bone morphogenetic protein (BMP) receptor type II (BMPR2) (Invitrogen; Thermo Fisher Scientific, cat. no. MA5-15827, 1:1000 dilution), transforming growth factor β (TGF-β) (Abcam, Cambridge, UK, cat. no. ab215715, 1:1000 dilution), α-SMA (Abcam, cat. no. ab32575, 1:1000 dilution) Pan acetyl-lysine (Abcam, cat. no. ab21623, 1:1000 dilution), HA-tag (Sigma-Aldrich; Merck KGaA, cat. no. H3663, 1:2000 dilution), FLAG-tag (Sigma-Aldrich; Merck KGaA, cat. no. F3165, 1:2000 dilution), Myc-tag (Abcam, cat. no. ab32, 1:2000 dilution), glyceraldehyde-3-phosphate dehydrogenase (GAPDH) (Beyotime Institute of Biotechnology, cat. no. AG019, 1:3000 dilution), and α-tubulin (Beyotime Institute of Biotechnology, cat. no. AT819, 1:3000 dilution).

2.15 Statistical analysis

Microsoft Excel was used for statistical analysis. All cell experiment data are presented as means ± Std.error (SEM). Shapiro–Wilk test was used for testing the normality of datasets and the Brown–Forsythe test for equal variance. For data with normal distribution, a two-tailed Student *t*-test was used to compare differences in two groups and two-way analysis of variance (ANOVA) with Holm-Šídák's post-hoc test for multiple groups. For non-normally distributed data or data with a small sample size ($n < 6$), the Mann–Whitney *U* test and Kruskal–Wallis with Dunn post-hoc test were used to compare differences among two groups and multiple groups. $*P < 0.05$, $**P < 0.01$, and $***P < 0.001$ (two-tailed) was considered statistically significant.

3. Results

3.1 Decreased SIRT7 expression promotes PH pathogenesis

To investigate the role of SIRT7 in PH pathogenesis, we first analysed its mRNA levels in two Gene Expression Omnibus (GEO) databases from patients with PH.[26,27] These datasets are lung tissues taken from 15 PAH patients and 11 healthy individuals (GSE113439) and the transcriptomic profiles of lung tissues from 58 patients with PAH vs. 25 healthy controls (HC) (GSE117261). *SIRT7* mRNA levels were significantly downregulated in lung tissues of PAH patients (*Figure 1A*), while *SIRT1-6* mRNA levels did not differ significantly between the groups (see Supplementary material online, *Figure S1*). To confirm this finding, we generated a SuHx-induced PH mouse model. Consistently, *Sirt7* mRNA and protein levels were significantly reduced in the murine lung tissues (*Figure 1B*). Next, to determine whether SIRT7 downregulation exacerbated PH or

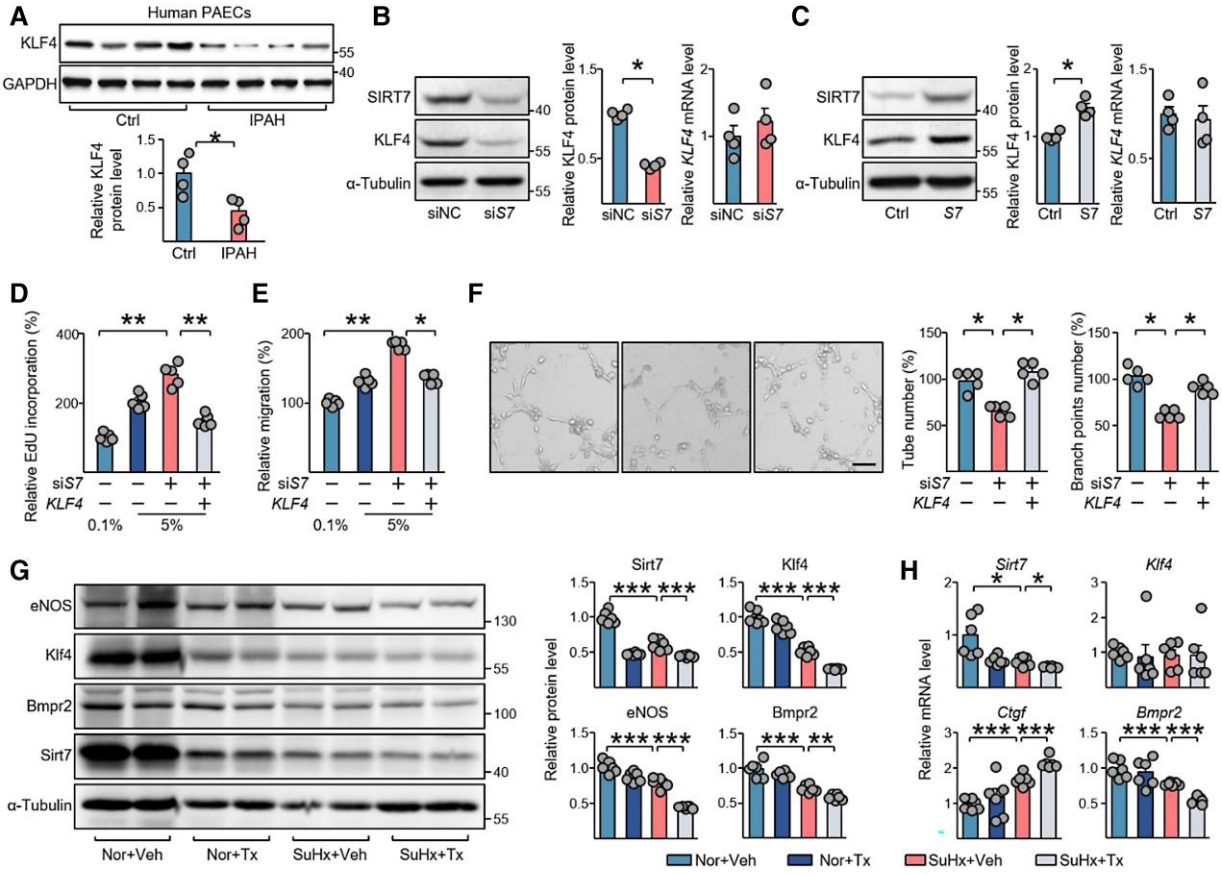

Figure 4 SIRT7 regulates PAEC function via KLF4. (*A*) Immunoblotting analysis of KLF4 protein levels in PAECs isolated from IPAH patients (IPAH, $n = 4$) and control individuals (Ctrl, $n = 4$). (*B*) PAECs were transfected with siRNA against *SIRT7* (si*S7*, 20 nM) or control siRNA (siNC, 20 nM) for 48 h. Protein levels of SIRT7 and KLF4 were detected by western blotting analysis, and RNA levels of KLF4 were measured by real-time qPCR. (*C*) PAECs were infected with *SIRT7* lentivirus (*S7*) or control lentivirus (Ctrl) for 48 h. Protein levels of SIRT7 and KLF4 were detected by Western blotting analysis, and KLF4 mRNA level was measured by real-time-qPCR. (*D–F*) PAECs were transfected with control siRNA (siNC, 20 nM) or si*SIRT7* (si*S7*, 20 nM) for 24 h, then transfected with KLF4 plasmid (*KLF4*, 2 μg/mL) or vehicle plasmid (2 μg/mL) for 48 h. Proliferation of PAECs was measured by EdU incorporation (*D*); migration of PAECs was detected by wound healing assays (*E*); and angiogenesis ability of PAECs was measured by tube formation assays (*F*). Scale bar = 20 μm (*F*). (*G*, *H*) Eight-week-old *Sirt7*$^{f/f}$; Cdh5-Cre^{ERT} mice challenged with Tx or vehicle (Veh) were exposed to normoxia (Nor) or SuHx model for 4 weeks. (*G*) Western blotting analysis of Sirt7, Klf4, eNOS, and Bmpr2 protein levels, and (*H*) qPCR analysis of *Sirt7*, *Klf4*, *Ctgf*, and *Bmpr2* mRNA levels in lung tissues of indicated groups of mice. Data are means ± SEM. Four independent experiments in (*B*, *C*) and five independent experiments in (*D–F*) were performed. Data are of six mice per group (*G*, *H*). Data were analysed by Mann–Whitney *U* test (*A–C*), and by Kruskal–Wallis test with Dunn post-hoc test in (*D–F*). Data were analysed by two-way ANOVA with Holm-Šídák's post-hoc test (*G*, *H*). $^*P < 0.05$, $^{**}P < 0.01$, $^{***}P < 0.001$ with comparisons indicated by lines.

represented a consequence of PH, we examined SuHx-induced PH features in *Sirt7*-KO mice. The *Sirt7*-KO mice developed more severe PH phenotypes than wild-type (WT) controls, as evidenced by increased RVSP, Fulton Index, and pulmonary artery wall thickness (*Figure 1C–E*). To investigate whether *Sirt7* loss exacerbated PH due to systemic defects, we used a recombinant adeno-associated virus type 1 vector harbouring an sh*Sirt7*-interfering RNA cassette. Mice were intratracheally treated with sh*Sirt7* to knock down *Sirt7* in the lungs and then treated with SuHx. *Sirt7* was successfully knocked down in lung tissues (see Supplementary material online, *Figure S2*). *Sirt7* knockdown led to more severe PH as compared with scramble controls, as evidenced by increased RVSP and Fulton Index (*Figure 1F* and *G*). In addition, pulmonary arterial wall thickness and small vascular remodelling, both hallmarks of PH, were also increased by *Sirt7* deficiency (*Figure 1H* and *I*). Taken together, these results suggest that SIRT7 loss is involved in the development of PH.

3.2 Endothelial-specific deletion of *Sirt7* exacerbates PH

Endothelial dysfunction is a critical initiating factor in PH.[4] To study the role of endothelial SIRT7 in PH, we examined the expression of SIRT7 in lung biopsies collected from IPAH patients and controls. An obvious reduction of SIRT7 level in pulmonary endothelium was demonstrated by immunostaining (*Figure 2A*). Furthermore, we determined the SIRT7 level in PAECs isolated from 4 IPAH patients. Western blotting analysis confirmed the significant decrease in SIRT7 level in IPAH PAECs as compared with healthy control PAECs (*Figure 2B*). When exposed to hypoxia, SIRT7 mRNA and protein levels were reduced in PAECs (see Supplementary material online, *Figure S3A and B*). >HIF-2α has been reported to be specifically induced by hypoxia in PAECs.[28] We found that overexpression of HIF-2α suppressed SIRT7 expression, while knockdown of HIF-2α abolished the suppression of SIRT7 by hypoxia (see Supplementary material online, *Figure S3C–F*).

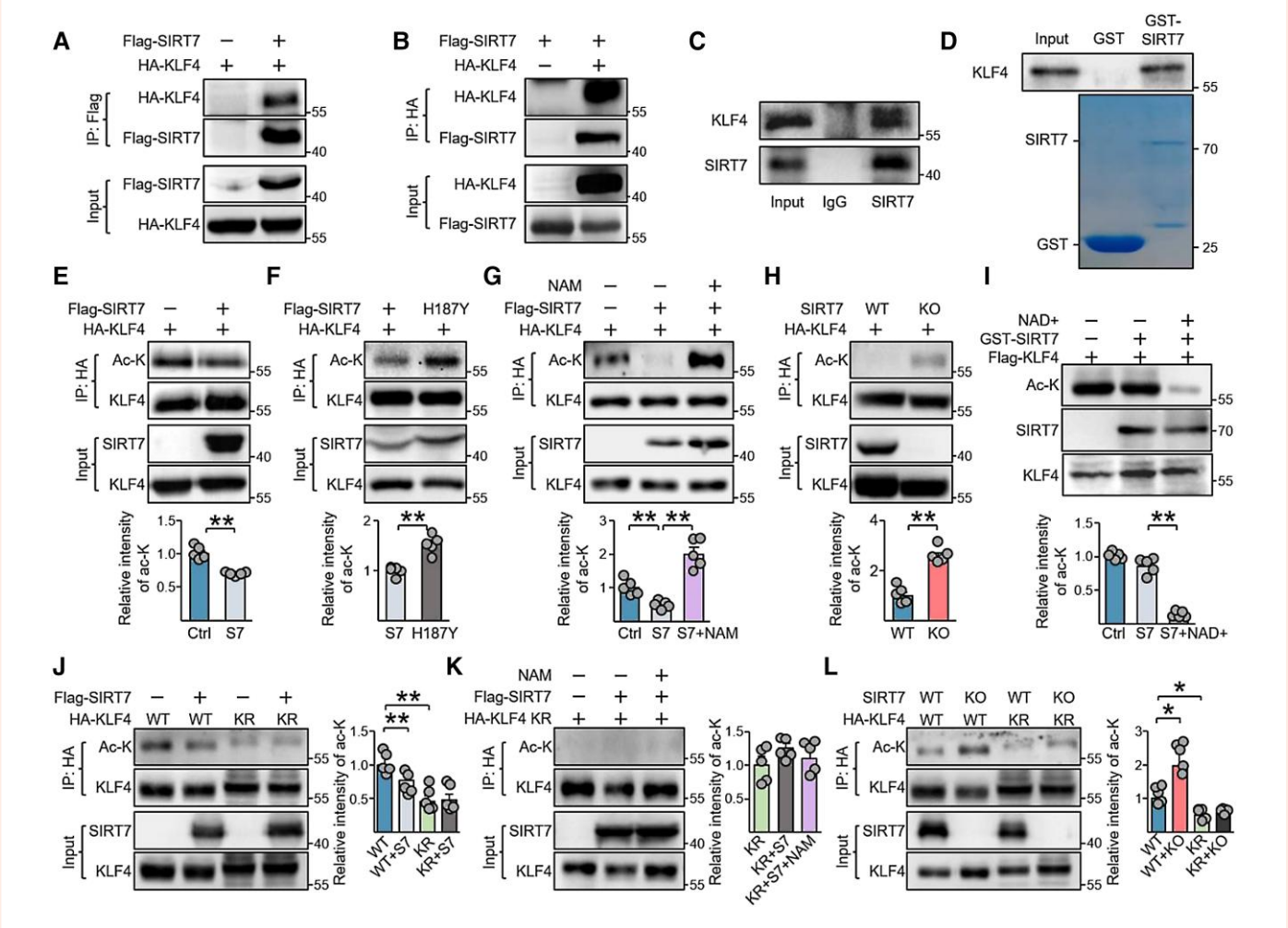

Figure 5 SIRT7 interacts with and deacetylates KLF4 at K228. (*A*, *B*) FLAG-SIRT7 and HA-KLF4 were co-expressed in HEK293T cells for 48 h. Immunoblots showing the presence of (*A*) HA-KLF4 in anti-Flag immunoprecipitates and (*B*) FLAG-SIRT7 in anti-HA immunoprecipitates. (*C*) Western blotting of the protein level of endogenous KLF4 and SIRT7 in anti-SIRT7 immunoprecipitates from PAECs. IgG was a control antibody. (*D*) GST pull-down assay was performed to test the *in vitro* binding of purified Flag-KLF4 and GST-fused SIRT7 from *E. coli.* Coomassie blue staining showing the levels of GST and GST-SIRT7. (*E*, *F*) HA-KLF4 was co-expressed with SIRT7 (*E*) or SIRT7-H187Y (*F*) for 48 h in HEK293T cells. KLF4 acetylation was measured in anti-HA immunoprecipitates. (*G*) Western blotting showing the acetylation levels of KLF4 in the presence of SIRT7, with or without NAM (10 mM, 24 h) treatment. (*H*) Immunoblots showing the acetylation levels of KLF4 in control HEK293T cells (WT) or *SIRT7*-KO HEK293T cells. (*I*) Purified FLAG-KLF4 was incubated with GST-SIRT7 with or without NAD^+ (1 mM). KLF4 acetylation was measured with anti-pan acetyl-lysine. (*J*) Representative immunoblots showing the acetylation levels of KLF4 WT and KLF4-K228R (KR) in the absence or presence of SIRT7. (*K*) KLF4-K228R acetylation levels in the presence of SIRT7, with or without NAM treatment for 24 h. (*L*) Representative immunoblots showing the acetylation levels of KLF4 WT and KLF4-K228R (KR) in control HEK293T cells (WT) or *SIRT7*-KO HEK293T cells. Three independent experiments were performed (*A*–*D*). Data are means ± SEM from five independent experiments (*E*–*L*), and were analysed by Mann–Whitney *U* test (*E*, F, *H*) and Kruskal–Wallis test with Dunn post-hoc test (*G*, *I*–*L*). $^*P < 0.05$, $^{**}P < 0.01$ with comparisons indicated by lines.

We then examined the causal association of SIRT7 with pulmonary endothelial function during PH by generating a *Sirt7*$^{f/f}$; Cdh5-cre/ERT mouse line with EC-specific *Sirt7* KO induced by tamoxifen (Tx). The absence of SIRT7 protein in lung ECs was validated (*Figure 2C*). When challenged with SuHx, EC ablation of *Sirt7* exacerbated the PH phenotype in mice, as evidenced by increased RVSP, Fulton Index, pulmonary arterial vascular wall thickness, and remodelling (*Figure 2D–G*). Because *Sirt7*$^{f/f}$; Cdh5-cre/ERT mice treated with TX led to global depletion of *Sirt7* in the endothelium. We next generated an rAAV-*ICAM2-Cre* vector (ICre) with a synthetic *ICAM2* promoter-driven *Cre* recombinase expressing cassette. *Sirt7*$^{f/f}$ mice were challenged with inhalation of these viral particles to drive *Sirt7* deletion in pulmonary endothelium. As shown, Sirt7 level was significantly lower in isolated pulmonary ECs from ICre-inhaled mice than in control ECs (see Supplementary material online, *Figure S4A*). When exposed to SuHx, mice receiving ICre displayed a more severe PH phenotype, as evidenced by increased RVSP, Fulton Index, and pulmonary arterial vascular wall thickness and damaged vascular system (see Supplementary material online, *Figure S4B–E*). Together, these data suggest a causal role of SIRT7 loss in pulmonary endothelium in PH pathogenesis.

3.3 SIRT7 maintains pulmonary arterial EC function via KLF4

PH is characterized by increased PAEC proliferation and migration, but the homeostatic function of these ECs is impaired.[3,4] To examine the

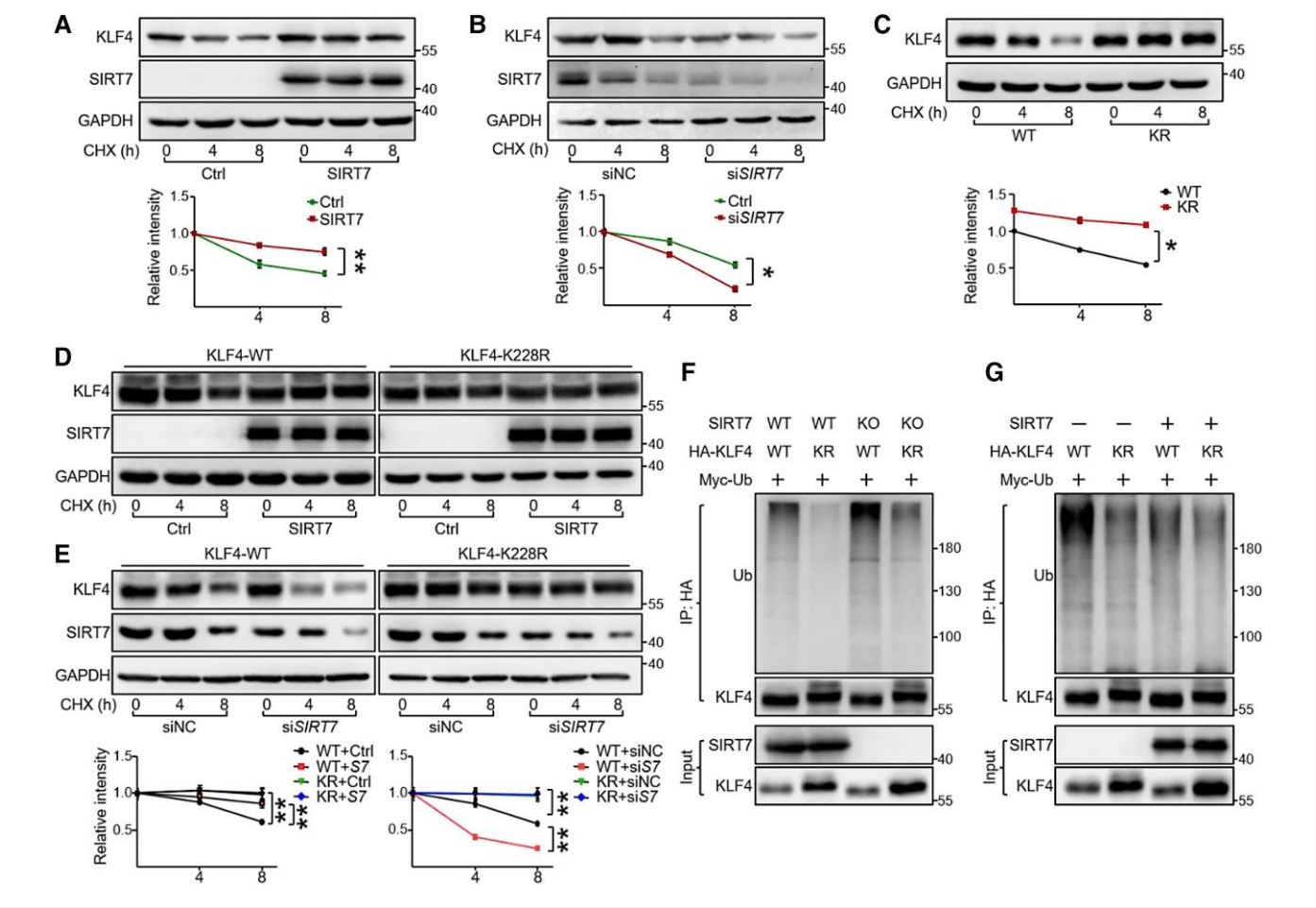

Figure 6 SIRT7-associated deacetylation of KLF4 promotes protein stability. (*A*, *B*) Western blotting analysis of KLF4 protein levels in PAECs overexpressing SIRT7 (*A*), transfected with si*SIRT7* (20 nM) (*B*) or control siRNA (siNC, 20 nM) for 48 h, and then treated with CHX (50 μg/mL) for 0, 4, and 8 h. (*C*) Western blotting analysis of KLF4 protein levels in HEK293T cells overexpressing KLF4 or KLF4-K228R for 48 h then treated with CHX for 0, 4, and 8 h. (*D*, *E*) Western blotting analysis of KLF4 or KLF4-K228R protein levels in HEK293T cells with SIRT7 overexpression (*D*) or knockdown (*E*). (*F*, *G*) Western blotting analysis of ubiquitination of KLF4 protein in *SIRT7*-KO HEK293T cells (*F*) and SIRT7-overexpressing HEK293T cells (*G*) transfected with KLF4 plasmid (2 μg/mL) or KLF4 K228R plasmid (2 μg/mL) for 48 h. Data are means ± SEM from five independent experiments. Data are analysed by Mann–Whitney *U* test (*A*–*C*) and Kruskal–Wallis test with Dunn post-hoc test (*D*, *E*). $^{*}P < 0.05$, $^{**}P < 0.01$ with comparisons indicated by lines.

regulatory role of SIRT7 in pulmonary endothelial function, we cultured PAECs and knocked down *SIRT7* via siRNA. PAEC proliferation and migration was significantly increased, and tube formation ability was suppressed (*Figure 3A–C*). In contrast, lentivirus-mediated overexpression of *SIRT7* inhibited the proliferation and migration of PAECs and improved tube formation ability (*Figure 3D–F*). Next, we determined the expression of PH-associated genes in PAECs by real-time qPCR. The mRNA expression of pro-PH genes, including transforming growth factor β1 (*TGFB1*), connective tissue growth factor (*CTGF*), *IL-6*, *IL-1B*, and endothelin-1 (*EDN1*) were all upregulated with *SIRT7* knockdown; the mRNA level of the anti-PH gene BMP receptor type II (*BMPR2*) was suppressed with *SIRT7* knockdown (*Figure 3G*). In contrast, *SIRT7* overexpression in PAECs reduced *TGFB1*, *CTGF*, *IL-6*, *IL-1B*, and *EDN1* mRNA levels, but increased *BMPR2* mRNA levels (*Figure 3H*). Western blotting analysis suggested that *SIRT7* knockdown impaired endothelial function, with decreased expression of eNOS and BMPR2 but increased the expression of TGF-β and α-SMA (*Figure 3I*). In complementary experiments, *SIRT7* overexpression upregulated eNOS and BMPR2 while downregulating TGF-β in PAECs (*Figure 3J*).

Next, we examined the underlying mechanisms by which SIRT7 regulates PAEC function. We analysed gene expression profiles in lung tissues from patients with PAH (GSE117261) and identified the 28 most downregulated genes (fold change in expression <0.5) (see Supplementary material online, *Table S3*). We used these data to predict potential transcription factor binding sites. Among the top-ranked transcription factors, KLF4 is closely associated with endothelial homeostasis and PH[21,22] (see Supplementary material online, *Figure S5*). Although *KLF4* mRNA levels were reduced in lung tissues of PAH/IPAH patients in the GSE117261 data set, they were not significantly altered, in comparison with controls in the GSE113439 data set (see Supplementary material online, *Figure S6*). We then analysed the protein level of KLF4 in PAECs from human IPAH. KLF4 level was greatly suppressed in IPAH PAECs as compared with controls (*Figure 4A*). We also analysed KLF4 level in cultured PAECs with *SIRT7* knockdown and found KLF4 level indeed attenuated in *SIRT7*-knockdown PAECs, with only slight change in mRNA level (*Figure 4B*). Moreover, *SIRT7* overexpression in PAECs significantly increased KLF4 protein level (*Figure 4C*), and *KLF4* overexpression abolished the proliferative and migrative abilities of cells (*Figure 4D* and *E*), but increased tube formation in *SIRT7*-knockdown

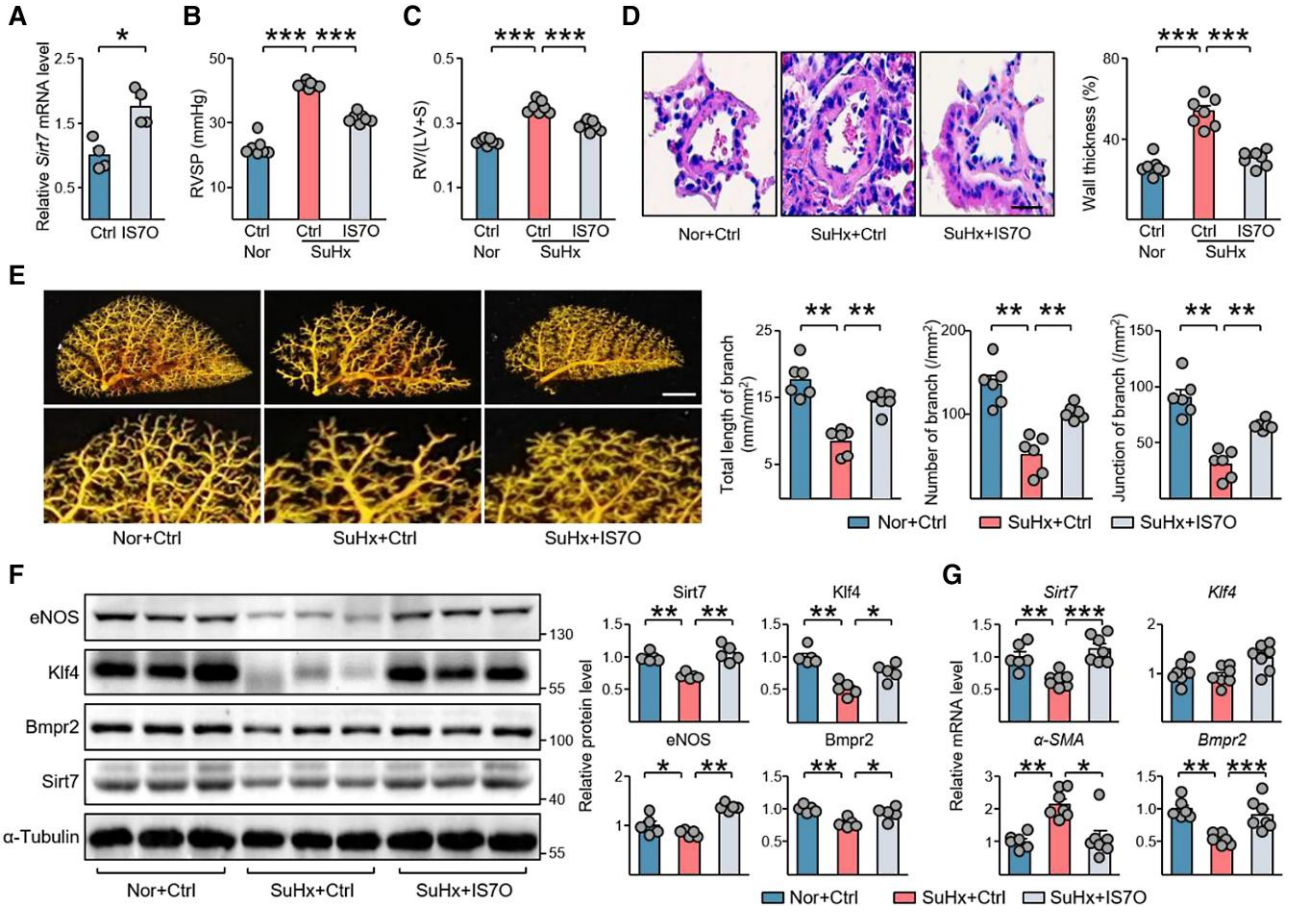

Figure 7 Endothelial cell-specific *Sirt7* delivery protects against PH pathogenesis. (*A*) qPCR analysis of *Sirt7* mRNA levels in mouse lung ECs after inhalation of rAAV-IS7O ($n = 4$) and control AAV (Ctrl, $n = 4$). (*B–E*) Eight-week-old mice were intratracheally inhaled with rAAV-*IS7O* or control AAV. Two weeks later, mice were exposed to normoxia or SuHx for 4 weeks. (*B*) RVSP and (*C*) Fulton Index were measured. Vascularization was shown by (*D*) H&E staining and (*E*) angiography. Scale bar = 20 μm (*D*) and 1 mm (*E*). (*F*) Western blotting analysis of Sirt7, Klf4, eNOS, and Bmpr2 protein levels in mice lung tissues of indicated groups. (*G*) qPCR analysis of *Sirt7*, *Klf4*, *α-SMA*, and *Bmpr2* mRNA levels in lung tissues of indicated groups. Data are means ± SEM (five–seven mice per group). Data were analysed using (*A*) Mann–Whitney *U* test, and (*B–G*) Kruskal–Wallis test with Dunn post-hoc test. *$P < 0.05$, **$P < 0.01$, ***$P < 0.001$ with comparisons indicated by lines.

PAECs (*Figure 4F*). The expression of pro-PH genes (*CTGF*, *IL-6* and *IL-1B*) caused by *SIRT7* knockdown was also restored by overexpression of *KLF4* (see Supplementary material online, *Figure S7*). We further studied the effect of the SIRT7/KLF4 axis *in vivo*. As shown, *Sirt7* depletion in ECs suppressed Klf4, eNOS, and Bmpr2 expression in lung tissues of *Sirt7*$^{f/f}$; Cdh5-cre/ERT mice treated with TX (*Figure 4G* and *H*) and *Sirt7*$^{f/f}$ mice inhaled with ICre (see Supplementary material online, *Figure S8*) as compared with controls. In addition, PH mice with *Sirt7* knockdown or *Sirt7* KO exhibited lower levels of eNOS, Klf4, and Bmpr2 as compared with controls (see Supplementary material online, *Figure S9*). Notably, little change was observed in the expression of *VEGF*, VEGF receptor 2 (*VEGFR2*), or *HIF1A* after *SIRT7* manipulation (see Supplementary material online, *Figure S10*). Thus, these results suggest that SIRT7 maintains PAEC function via KLF4.

3.4 SIRT7 deacetylates and stabilizes KLF4

We next investigated mechanisms by which SIRT7 regulates KLF4. We performed Co-IP assays to detect potential interactions between SIRT7 and KLF4 in HEK293T cells that ectopically expressed HA-KLF4 with FLAG-SIRT7 or vector control. HA-KLF4 protein expression was detected in anti-FLAG immunoprecipitates from FLAG-SIRT7 transfected cells by Western blotting but not those transfected with the vector control (*Figure 5A*). Likewise, FLAG-SIRT7 was detected in anti-HA immunoprecipitates in cells transfected with HA-KLF4 but not in cells transfected with the vector control (*Figure 5B*). In addition, endogenous KLF4 expression was shown in anti-SIRT7 PAEC immunoprecipitates (*Figure 5C*). The results of GST-pull-down assays also suggested that SIRT7 interacted with KLF4 (*Figure 5D*).

Given that SIRT7 is a deacetylase, we investigated whether KLF4 represents a target of SIRT7 deacetylation. To that end, we overexpressed HA-KLF4 with WT SIRT7 or the catalytic-deficient SIRT7-H187Y in HEK293T cells and detected acetyl-lysine levels in anti-HA-KLF4 immunoprecipitates. Overexpression of SIRT7-WT but not SIRT7-H187Y reduced the level of acetylated-KLF4 (*Figure 5E* and *F*). Furthermore, the inhibition of SIRT7 with NAM, a pan sirtuin inhibitor, abolished SIRT7-associated KLF4 deacetylation (*Figure 5G*). As well, *SIRT7* deletion in HEK293T cells resulted in increased KLF4 acetylation (*Figure 5H*). Consistently, the acetylation of endogenous KLF4 in PAECs was significantly reduced in SIRT7-WT- but not SIRT7-H187Y-overexpressing cells, and inhibition of SIRT7 using siRNA or NAM increased KLF4 acetylation (see Supplementary material online, *Figure S11*). In addition, *in vitro* deacetylation assay revealed that GST-SIRT7 reduced KLF4 acetylation only in the presence of NAD^+ (*Figure 5I*).

To identify the deacetylation sites of KLF4 that were targeted by SIRT7, we constructed 3 truncated KLF4 forms and found that only

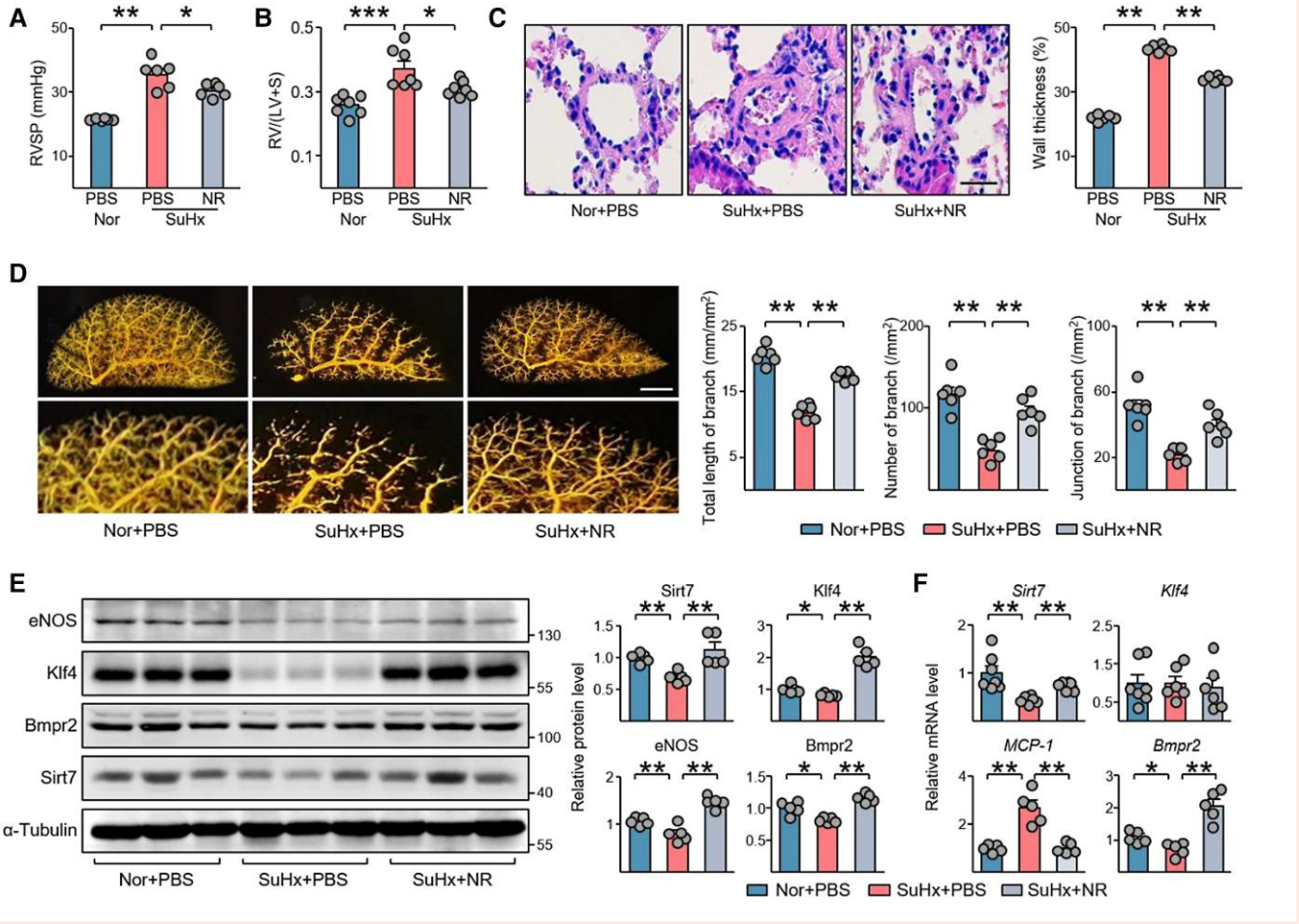

Figure 8 NAM riboside (NR) treatment reverses PH phenotypes in a rodent model. (*A*, *B*) Eight-week-old mice were exposed to normoxia (Nor) or SuHx for 4 weeks, followed by oral delivery of NR (400 mg/kg/day) or PBS daily for the last week. (*A*) RVSP and (*B*) Fulton Index were measured. (*C*) H&E staining showing PA wall thickness in the indicated groups. Scale bar = 20 μm. (*D*) Angiography showing the vascular structure of left lung tissues. Scale bar = 1 mm. (*E*) Western blotting analysis of Sirt7, Klf4, eNOS, and Bmpr2 proteins, and (*F*) qPCR analysis of *Sirt7*, *Klf4*, *MCP-1*, and *Bmpr2* mRNA levels in lung tissues of indicated groups. Data are means ± SEM (five–seven mice per group). Data were analysed by Kruskal–Wallis test with Dunn post-hoc test. $*P < 0.05$, $**P < 0.01$, and $***P < 0.001$ with comparisons indicated by lines.

the intermediate region could be acetylated (see Supplementary material online, *Figure S12A*). KLF4 intermediate region acetylation was suppressed with SIRT7 overexpression (see Supplementary material online, *Figure S12B and C*). KLF4 has also been reported to be acetylated by p300/cyclic-AMP response element binding protein binding protein (CBP)-associated factor (PCAF) at lysine 228 (K228), which is in the intermediate region.[29] We reasoned that SIRT7 may also target K228 of KLF4. PCAF overexpression-induced acetylation of KLF4 was abolished by SIRT7 overexpression, but not by overexpression of its mutated form H187Y (see Supplementary material online, *Figure S13A*). Next, we generated a KLF4 deacetylation mimic by replacing lysine 228 with arginine (K228R). Acetylation was reduced in HA-KLF4-K228R as compared with the WT, and neither PCAF nor SIRT7 overexpression affected HA-KLF4-K228R acetylation (see Supplementary material online, *Figure S13B and C*, *Figure 5J*). Likewise, neither NAM treatment nor *SIRT7*-KO affected HA-KLF4-K228R acetylation (*Figure 5K* and *L*). Together, these data suggest that SIRT7 deacetylates KLF4 at K228.

Because *SIRT7* knockdown (KD) reduced KLF4 levels in PAECs, and *SIRT7* overexpression increased KLF4 levels, we investigated whether SIRT7 might regulate KLF4 protein stability. Using cycloheximide to inhibit protein synthesis, we found that degradation of endogenous KLF4 in PAECs was inhibited by SIRT7 overexpression but was promoted otherwise by *SIRT7* deprivation (*Figure 6A* and *B*). In addition, the degradation of KLF4-K228R mutants was delayed as compared with the WT (*Figure 6C*). The degradation of HA-KLF4 was also inhibited by SIRT7 overexpression but was increased by si*SIRT7* transfection. However, the degradation of KLF4-K228R was not affected by SIRT7 overexpression or knockdown (*Figure 6D* and *E*). Next, we investigated whether SIRT7 increased KLF4 protein stability by inhibiting ubiquitination, because ubiquitination has been reported to be the main KLF4 degradation mechanism.[30] SIRT7 overexpression suppressed polyubiquitination of KLF4, but its deletion or knockdown increased KLF4 ubiquitination (*Figure 6F* and Supplementary material online, *Figure S14A*). Consistently, ubiquitination was reduced in K228R mutants but not K228Q mutants as compared with WT KLF4 (see Supplementary material online, *Figure S14B*). SIRT7 overexpression or deletion had no additional effect on the mutants (*Figure 6F* and *G*).

3.5 Endothelial-specific *Sirt7* delivery ameliorates PH in a rodent model

Next, we explored the therapeutic potential of SIRT7 in the treatment of PH by using an inducible *Sirt7*-transgenic mouse line (*Sirt7*-Tg),[16] in which Sirt7 overexpression is induced by doxycycline (Dox). Dox-fed *Sirt7*-Tg

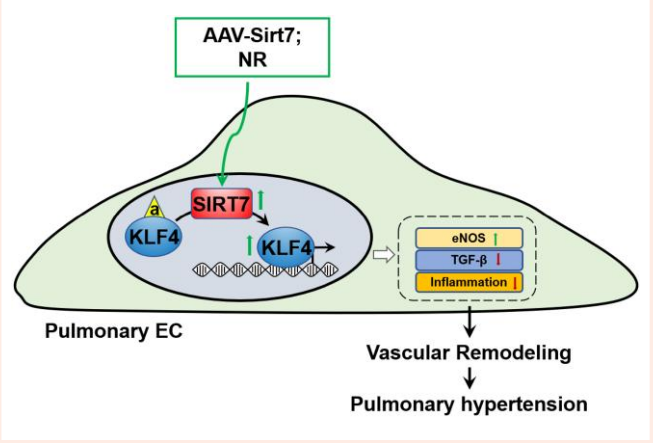

Figure 9 Targeting endothelial SIRT7 as a therapeutic strategy for PH. SIRT7 deacetylates and thus maintains KLF4 protein levels. Targeting the pulmonary endothelium via AAV-mediated delivery and NR-induced activation of Sirt7 alleviates PH in mice, providing an optimistic novel therapeutic strategy for PH.

mice displayed an ameliorated PH phenotype as compared with Dox-fed WT mice when challenged with SuHx, as evidenced by reduced RVSP, Fulton Index and vascular remodelling (see Supplementary material online, *Figure S15A–C*). Klf4 and the expression of other PH-associated genes were also restored in *Sirt7*-Tg mice as compared with controls (see Supplementary material online, *Figure S15D and E*).

Next, we treated SuHx-PH mice with inhalation of endothelial-specific targeting rAAV- IS7O or control AAVs. RVSP and right ventricular hypertrophy were induced in mice exposed to SuHx treatment, and IS7O delivery markedly reduced RVSP and Fulton Index (*Figure 7A–C*). Pulmonary vascular remodelling and vascular structure damage were also suppressed by this endothelial-specific *Sirt7* delivery, as revealed by H&E staining and angiograms, respectively (*Figure 7D* and *E*). Klf4 and its downstream gene eNOS, as well as anti-PH Bmpr2, were upregulated in SuHx + IS7O mouse lung tissues (*Figure 7F* and *G*). Acetylation and ubiquitination of Klf4, which was upregulated in SuHx-PH mouse lungs, were suppressed by *Sirt7* delivery (see Supplementary material online, *Figure S16*). Furthermore, PH-associated genes, including *MCP-1*, nucleotide-binding domain and leucine-rich repeat (LRR)-containing (NLR) family pyrin domain containing 3 (*Nlrp3*), *Il-6*, *Il-1b*, angiopoietin 1 (*Angpt1*), and *Edn1*, were suppressed by *Sirt7* (see Supplementary material online, *Figure S17*).

3.6 NAM riboside (NR) supplementation rescues PH pathogenesis

The NAD^+ intermediate NR upregulates NAD^+ levels in various tissues and improves physiological functions in both aged humans and mice.[31,32] We orally administered NR (400 mg/kg/day) to SuHx-induced PH mice daily for 1 week, with PBS as a control. Haemodynamic analysis suggested that NR treatment significantly reduced RVSP and Fulton index in PH mice (*Figure 8A* and *B*). Pulmonary vascular wall thickness and remodelling were also improved by NR treatment (*Figure 8C* and *D*). Furthermore, the Sirt7/Klf4 axis was activated in SuHx + NR mouse lung tissues as compared with the control (*Figure 8E* and *F*). Further, we treated pulmonary EC-specific *Sirt7*-deficient mice with NR. In the presence of NR, Sirt7 deletion increased the PH susceptibility, as indicated by increased RVSP and Fulton Index in the SuHx + ICre + NR vs. SuHx + Ctrl + NR group (see Supplementary material online, *Figure S18*).

Collectively, these results demonstrated that the expression of both SIRT7 and KLF4 was reduced in the pulmonary endothelium of IPAH patients and lung tissues of PH mice. SIRT7 deacetylated KLF4 at lysine 228 to enhance KLF4 protein stability. Using *Sirt7*-KO and transgenic mice, as well as IS7O particles and NR feeding, we showed that EC-specific SIRT7 targeting ameliorates PH and represents a novel therapeutic strategy for treating PH (*Figure 9*).

4. Discussion

Pulmonary endothelial dysfunction has emerged as a potential novel therapeutic target for treating PH, a disease that occurs prevalently in older people. NAD^+-dependent sirtuins are among the most targetable genes/pathways known to improve health and longevity.[10] With reduced NAD^+ levels during aging, sirtuin levels and functions are diminished in senescent organisms.[9] Here, we characterized a pathophysiological mechanism of endothelial damage during PH. Mainly, reduced SIRT7 expression was associated with PH pathogenesis in humans and animal models. Both lung tissue- and endothelial-specific *Sirt7* depletion exacerbated PH development. For translational implications, the endothelial-specific delivery of the *Sirt7* gene via AAV alleviated the pathological features of PH, which confirms that pulmonary endothelial dysfunction is a potential target for PH treatment.

NAD^+ fuels cellular biological processes and decreased NAD^+ levels are commonly found in older mammals.[9] Oral delivery of NR improved skeletal muscle function in aged mice and extended their lifespan.[31] Although the expression of NAM phosphoribosyltransferase (NAMPT), a rate-limiting enzyme in NAD biosynthesis, is increased in PH animal models and patients, the beneficial effect of NAMPT inhibition likely increases the proliferation of PASMCs via store-operated calcium entry (SOCE), instead of NAD^+ production.[33] Here, we showed that NR supplementation, by increasing NAD^+ levels, ameliorated PH symptoms in animal models. However, this benefit was largely blunted by *Sirt7* deficiency, which further suggests the pivotal role of SIRT7 in PH. Thus, NR treatment may represent a new therapeutic strategy for PH.

SIRT7 is localized in the nucleus, where it deacetylates and thus regulates the function of histones and various transcription factors.[18,34] *Sirt7* deficiency causes premature aging in mice, whereas AAV-mediated *Sirt7* overexpression ameliorates vascular senescence and inflammation, hence extending the lifespan of murine progeria models.[18,35] In acute lung injury, *Sirt7* deficiency promotes endothelial-to-mesenchymal transition and the permeability of primary pulmonary ECs.[20] These features are common to damaged ECs involved in PH. The protective role of endothelial KLF4 is well documented in various cardiovascular diseases, including atherosclerosis, coronary injury, cerebral vascular injury, and PH.[21,22,36,37] Mechanistically, KLF4 activates *NOS3* transcription while suppressing the nuclear factor (NF)-κB-dependent inflammatory pathway in ECs.[38,39] In this study, we identified that the SIRT7/KLF4 axis is a critical regulator of PH. Initially, we characterized the post-translational regulation of KLF4 during PH pathogenesis. KLF4 can be acetylated by p300 and PCAF, and deacetylated by HDAC2 and SIRT1.[29,40–42] However, the dynamic acetylation status of KLF4 involved in PH pathogenesis remains unclear. We demonstrated that SIRT7 interacted with KLF4 and regulated its acetylation, thus regulating its stability. Given that KLF4 is an important transcription factor in ECs, the anti-inflammatory effects of SIRT7 in vascular function may be mediated by KLF4 K228 deacetylation. KLF4 stability was found regulated by the E3 ligase Mule and the deubiquitinase USP10[43,43] Further study is warranted to clarify whether Mule or USP10 are involved in SIRT7-mediated KLF4 stability. Of note, KLF4 overexpression inhibited endothelial-to-mesenchymal transition by inducing microRNA-483.[44] Thus, SIRT7 may improve EC function during PH by KLF4-suppressed endothelial-to-mesenchymal transition.

HIFs and TGF-β signalling are known to participate in vascular injury and remodelling in PH.[3] HIF-1α and HIF-2α are differentially expressed in IPAH PASMCs and PAECs.[28] We found reduced SIRT7 expression in PAH PAECs might be due to hyperactivation of HIF-2α. The imbalance of TGF-β signalling caused by BMPR2 loss is involved in vascular remodelling during PH, and increased TGF-β level and Smad3 signalling activation were

observed in both PH patients and rodent models.[45,46] Our group previously found that TGF-β signalling inhibited *SIRT7* transcription and, conversely, SIRT7 deacetylated Smad4 to suppress TGF-β-induced epithelial-mesenchymal transition.[16,47]

Consistent with our study, recent studies found that pulmonary vascular senescence is pivotal in the pathogenesis of PH, with compromised endothelial function and vascular remodelling. Geroprotectors, SASP inhibitors, and senolytics were proven effective in the amelioration of PH.[5,6,48,49] Intriguingly, Born *et al.* demonstrated that the elimination of senescent pulmonary ECs by senolytics can worsen PH hemodynamics.[50] This seeming inconsistency is likely attributable to the different senolytic strategies, different senescence models, or different efficiency of endothelial rejuvenation after the clearance of senescent cells. In our study, compromised Sirt7/KLF4 axis in endothelium might couple cell senescence to PH pathogenesis. Here we targeted SIRT7 to improve endothelial function in pulmonary vessels rather than removing the senescent cells, which might serve as a new therapeutic choice.

In summary, the results of this study revealed that SIRT7 protects endothelial function via KLF4 deacetylation, maintaining normal vascular tone against PH pathogenesis. Endothelial-specific *Sirt7* gene delivery and Sirt7 activation by NR treatment ameliorated PH in a murine model, which casts light on a potential novel therapeutic target for PH, and represents an optimistic strategy for future preclinical and clinical treatment of this disease.

Translational perspective

Pulmonary endothelial cell dysfunction is pivotal in vascular remodelling process during pulmonary hypertension (PH) pathogenesis. We identified a SIRT7/KLF4 axis essential for pulmonary endothelial homeostasis, however compromised in PH patients and animal models. Pulmonary endothelium-specific *Sirt7* gene delivery or treatment with NAD^+ precursor reversed PH phenotypes, providing a new therapeutic strategy for PH.

Supplementary material

Supplementary material is available at *Cardiovascular Research* online.

Author Contribution

J.Z. and B.L. conceived the original idea and designed the overall experiments. J.Z., C.X., X.T., S.S., S.L., L.Y., Y.C., Q.Y., X.Y., L.Y., Y.N., and T.-Y.W.W. performed experiments. D.G. provided essential equipment. J.Z., C.X. and C.W. collected the data and performed statistical analysis. X.W., J.W., and J.Y.-J.S. contributed samples and provided essential input to the manuscript. J.Z., J.Y.-J.S., and B.L. wrote the manuscript. All authors give final approval of the version to be submitted.

Acknowledgements

The authors thank Prof. Jin-Song Bian (Southern University of Science and Technology) for kindly providing equipment, and Dr. Jessica Tamanini (Shenzhen University and ETediting) for editing the manuscript prior to submission.

Conflict of interest: none declared.

Funding

This work was supported by grants from the National Natural Science Foundation of China (grant nos. 82125012, 82061160495, 92249304, and 32090033 to B.L., 82100434 to J.Z. and 82170069 to Y.C.), the National Key R&D Program of China (2021ZD0202400 and 2023YFC2509902 to B.L.), the Guangdong Basic and Applied Research Foundation (2021B1515120062 to B.L.), and the Shenzhen Municipal Commission of Science and Technology Innovation (JCYJ20220818100016035 and JCYJ20220815150210001 to B.L.).

Data availability

The data underlying this article are available in the article and its online supplementary material.

References

1. Thenappan T, Ormiston ML, Ryan JJ, Archer SL. Pulmonary arterial hypertension: pathogenesis and clinical management. *BMJ* 2018;**360**:j5492.
2. Evans CE, Cober ND, Dai Z, Stewart DJ, Zhao YY. Endothelial cells in the pathogenesis of pulmonary arterial hypertension. *Eur Respir J* 2021;**58**:2003957.
3. Schermuly RT, Ghofrani HA, Wilkins MR, Grimminger F. Mechanisms of disease: pulmonary arterial hypertension. *Nat Rev Cardiol* 2011;**8**:443–455.
4. Budhiraja R, Tuder RM, Hassoun PM. Endothelial dysfunction in pulmonary hypertension. *Circulation* 2004;**109**:159–165.
5. van der Feen DE, Berger RMF, Bartelds B. Converging paths of pulmonary arterial hypertension and cellular senescence. *Am J Respir Cell Mol Biol* 2019;**61**:11–20.
6. Galiè N, Humbert M, Vachiery JL, Gibbs S, Lang I, Torbicki A, Simonneau G, Peacock A, Vonk Noordegraaf A, Beghetti M, Ghofrani A, Gomez Sanchez MA, Hansmann G, Klepetko W, Lancellotti P, Matucci M, McDonagh T, Pierard LA, Trindade PT, Zompatori M, HoeperM; ESC Scientific Document Group. 2015 ESC/ERS guidelines for the diagnosis and treatment of pulmonary hypertension. *Eur Heart J* 2016;**37**:67–119.
7. Minamino T, Komuro I. Vascular cell senescence: contribution to atherosclerosis. *Circ Res* 2007;**100**:15–26.
8. Culley MK, Zhao J, Tai YY, Tang Y, Perk D, Negi V, Yu Q, Woodcock CC, Handen A, Speyer G, Kim S, Lai YC, Satoh T, Watson AM, Aaraj YA, Sembrat J, Rojas M, Goncharov D, Goncharova EA, Khan OF, Anderson DG, Dahlman JE, Gurkar AU, Lafyatis R, Fayyaz AU, Redfield MM, Gladwin MT, Rabinovitch M, Gu M, Bertero T, Chan SY. Frataxin deficiency promotes endothelial senescence in pulmonary hypertension. *J Clin Invest* 2021;**131**:e136459.
9. Imai SI, Guarente L. It takes two to tango: NAD(+) and sirtuins in aging/longevity control. *NPJ Aging Mech Dis* 2016;**2**:16017.
10. Donmez G, Guarente L. Aging and disease: connections to sirtuins. *Aging Cell* 2010;**9**:285–290.
11. Zurlo G, Piquereau J, Moulin M, Da Silva J P, Gressette M, Ranchoux B, Garnier A, Ventura-Clapier R, Fadel E, Humbert M, Lemaire C, Perros F, Veksler V. Sirtuin 1 regulates pulmonary artery smooth muscle cell proliferation: role in pulmonary arterial hypertension. *J Hypertens* 2018;**36**:1164–1177.
12. Paulin R, Dromparis P, Sutendra G, Gurtu V, Zervopoulos S, Bowers L, Haromy A, Webster L, Provencher S, Bonnet S, Michelakis ED. Sirtuin 3 deficiency is associated with inhibited mitochondrial function and pulmonary arterial hypertension in rodents and humans. *Cell Metab* 2014;**20**:827–839.
13. Li L, Shi L, Yang S, Yan R, Zhang D, Yang J, He L, Li W, Yi X, Sun L, Liang J, Cheng Z, Shi L, Shang Y, Yu W. SIRT7 is a histone desuccinylase that functionally links to chromatin compaction and genome stability. *Nat Commun* 2016;**7**:12235.
14. Liu Z, Qian M, Tang X, Hu W, Sun S, Li G, Zhang S, Meng F, Cao X, Sun J, Xu C, Tan B, Pang Q, Zhao B, Wang Z, Guan Y, Ruan X, Liu B. SIRT7 couples light-driven body temperature cues to hepatic circadian phase coherence and gluconeogenesis. *Nat Metab* 2019;**1**:1141–1156.
15. Yamagata K, Yoshizawa T. Transcriptional regulation of metabolism by SIRT1 and SIRT7. *Int Rev Cell Mol Biol* 2018;**335**:143–166.
16. Tang X, Shi L, Xie N, Liu Z, Qian M, Meng F, Xu Q, Zhou M, Cao X, Zhu WG, Liu B. SIRT7 antagonizes TGF-β signaling and inhibits breast cancer metastasis. *Nat Commun* 2017;**8**:318.
17. Tang M, Li Z, Zhang C, Lu X, Tu B, Cao Z, Li Y, Chen Y, Jiang L, Wang H, Liu B, Xu X, Wang H, Zhu WG. SIRT7-mediated ATM deacetylation is essential for its deactivation and DNA damage repair. *Sci Adv* 2019;**5**:eaav1118.
18. Sun S, Qin W, Tang X, Meng Y, Hu W, Zhang S, Qian M, Liu Z, Cao X, Pang Q, Zhao B, Wang Z, Zhou Z, Liu B. Vascular endothelium-targeted sirt7 gene therapy rejuvenates blood vessels and extends life span in a Hutchinson-Gilford progeria model. *Sci Adv* 2020;**6**:eaay5556.
19. Wyman AE, Noor Z, Fishelevich R, Lockatell V, Shah NG, Todd NW, Atamas SP. Sirtuin 7 is decreased in pulmonary fibrosis and regulates the fibrotic phenotype of lung fibroblasts. *Am J Physiol Lung Cell Mol Physiol* 2017;**312**:L945–L958.
20. Wyman AE, Nguyen TTT, Karki P, Tulapurkar ME, Zhang CO, Kim J, Feng TG, Dabo AJ, Todd NW, Luzina IG, Geraghty P, Foronjy R, Hasday JD, Birukova AA, Atamas SP,

Birukov KG. SIRT7 deficiency suppresses inflammation, induces EndoMT, and increases vascular permeability in primary pulmonary endothelial cells. *Sci Rep* 2020;**10**:12497.
21. Yang C, Xiao X, Huang L, Zhou F, Chen LH, Zhao YY, Qu SL, Zhang C. Role of kruppel-like factor 4 in atherosclerosis. *Clin Chim Acta* 2021;**512**:135–141.
22. Shatat MA, Tian H, Zhang R, Tandon G, Hale A, Fritz JS, Zhou G, Martínez-González J, Rodríguez C, Champion HC, Jain MK, Hamik A. Endothelial Krüppel-like factor 4 modulates pulmonary arterial hypertension. *Am J Respir Cell Mol Biol* 2014;**50**:647–653.
23. Wang J, Niu N, Xu S, Jin ZG. A simple protocol for isolating mouse lung endothelial cells. *Sci Rep* 2019;**9**:1458.
24. Li G, Tang X, Zhang S, Jin M, Wang M, Deng Z, Liu Z, Qian M, Shi W, Wang Z, Xie H, Li J, Liu B. SIRT7 activates quiescent hair follicle stem cells to ensure hair growth in mice. *EMBO J* 2020; **39**:e104365.
25. Bailey TL, Elkan C. Fitting a mixture model by expectation maximization to discover motifs in biopolymers. *Pro Int Conf Intell Syst Mol Biol* 1994;**2**:28–36.
26. Mura M, Cecchini MJ, Joseph M, Granton JT. Osteopontin lung gene expression is a marker of disease severity in pulmonary arterial hypertension. *Respirology* 2019;**24**:1104–1110.
27. Stearman RS, Bui QM, Speyer G, Handen A, Cornelius AR, Graham BB, Kim S, Mickler EA, Tuder RM, Chan SY, Geraci MW. Systems analysis of the human pulmonary arterial hypertension lung transcriptome. *Am J Respir Cell Mol Biol* 2019;**60**:637–649.
28. Jiang L, Goncharov DA, Shen Y, Lin D, Chang B, Pena A, DeLisser H, Goncharova EA, Kudryashova TV. Akt-dependent glycolysis-driven lipogenesis supports proliferation and survival of human pulmonary arterial smooth muscle cells in pulmonary hypertension. *Front Med (Lausanne)* 2022;**9**:886868.
29. Zhang J, Xie M, Xia L, Yu T, He F, Zhao C, Qiu W, Zhao D, Liu Y, Gong Y, Yao C, Liu L, Wang Y. Sublytic C5b-9 induces IL-23 and IL-36a production by glomerular mesangial cells via PCAF-mediated KLF4 acetylation in rat Thy-1 nephritis. *J Immunol* 2018;**201**:3184–3198.
30. Wang X, Xia S, Li H, Wang X, Li C, Chao Y, Zhang L, Han C. The deubiquitinase USP10 regulates KLF4 stability and suppresses lung tumorigenesis. *Cell Death Differ* 2020;**27**: 1747–1764.
31. Elhassan YS, Kluckova K, Fletcher RS, Schmidt MS, Garten A, Doig CL, Cartwright DM, Oakey L, Burley CV, Jenkinson N, Wilson M, Lucas SJE, Akerman I, Seabright A, Lai YC, Tennant DA, Nightingale P, Wallis GA, Manolopoulos KN, Brenner C, Philp A, Lavery GG. Nicotinamide riboside augments the aged human skeletal muscle NAD(+) metabolome and induces transcriptomic and anti-inflammatory signatures. *Cell Rep* 2019;**28**:1717–1728.e6.
32. Cantó C, Houtkooper RH, Pirinen E, Youn DY, Oosterveer MH, Cen Y, Fernandez-Marcos PJ, Yamamoto H, Andreux PA, Cettour-Rose P, Gademann K, Rinsch C, Schoonjans K, Sauve AA, Auwerx J. The NAD(+) precursor nicotinamide riboside enhances oxidative metabolism and protects against high-fat diet-induced obesity. *Cell Metab* 2012;**15**:838–847.
33. Chen J, Sysol JR, Singla S, Zhao S, Yamamura A, Valdez-Jasso D, Abbasi T, Shioura KM, Sahni S, Reddy V, Sridhar A, Gao H, Torres J, Camp SM, Tang H, Ye SQ, Comhair S, Dweik R, Hassoun P, Yuan JX, Garcia JGN. Nicotinamide phosphoribosyltransferase promotes pulmonary vascular remodeling and is a therapeutic target in pulmonary arterial hypertension. *Circulation* 2017;**135**:1532–1546.
34. Tang M, Tang H, Tu B, Zhu WG. SIRT7: a sentinel of genome stability. *Open Biol* 2021;**11**: 210047.
35. Lagunas-Rangel FA. SIRT7 in the aging process. *Cell Mol Life Sci* 2022;**79**:297.
36. Yoshida T, Yamashita M, Horimai C, Hayashi M. Deletion of Krüppel-like factor 4 in endothelial and hematopoietic cells enhances neointimal formation following vascular injury. *J Am Heart Assoc* 2014;**3**:e000622.
37. Zhang X, Wang L, Han Z, Dong J, Pang D, Fu Y, Li L. KLF4 alleviates cerebral vascular injury by ameliorating vascular endothelial inflammation and regulating tight junction protein expression following ischemic stroke. *J Neuroinflam* 2020;**17**:107.
38. Huang Y, Han X, Tang J, Long X, Wang X. Salidroside inhibits endothelial–mesenchymal transition via the KLF4/eNOS signaling pathway. *Mol Med Rep* 2021;**24**:692.
39. Zhou G, Hamik A, Nayak L, Tian H, Shi H, Lu Y, Sharma N, Liao X, Hale A, Boerboom L, Feaver RE, Gao H, Desai A, Schmaier A, Gerson SL, Wang Y, Atkins GB, Blackman BR, Simon DI, Jain MK. Endothelial Kruppel-like factor 4 protects against atherothrombosis in mice. *J Clin Invest* 2012;**122**:4727–4731.
40. Evans PM, Zhang W, Chen X, Yang J, Bhakat KK, Liu C. Kruppel-like factor 4 is acetylated by p300 and regulates gene transcription via modulation of histone acetylation. *J Biol Chem* 2007;**282**:33994–34002.
41. Meng F, Han M, Zheng B, Wang C, Zhang R, Zhang XH, Wen JK. All-trans retinoic acid increases KLF4 acetylation by inducing HDAC2 phosphorylation and its dissociation from KLF4 in vascular smooth muscle cells. *Biochem Biophys Res Commun* 2009;**387**:13–18.
42. Zhang X, Chen J, Sun L, Xu Y. SIRT1 deacetylates KLF4 to activate Claudin-5 transcription in ovarian cancer cells. *J Cell Biochem* 2018;**119**:2418–2426.
43. Hao Z, Sheng Y, Duncan GS, Li WY, Dominguez C, Sylvester J, Su YW, Lin GH, Snow BE, Brenner D, You-Ten A, Haight J, Inoue S, Wakeham A, Elford A, Hamilton S, Liang Y, Zúñiga-Pflücker JC, He HH, Ohashi PS, Mak TW. K48-linked KLF4 ubiquitination by E3 ligase Mule controls T-cell proliferation and cell cycle progression. *Nat Commun* 2017;**8**:14003.
44. He M, Chen Z, Martin M, Zhang J, Sangwung P, Woo B, Tremoulet AH, Shimizu C, Jain MK, Burns JC, Shyy JY. miR-483 targeting of CTGF suppresses endothelial-to-mesenchymal transition: therapeutic implications in Kawasaki disease. *Circ Res* 2017;**120**:354–365.
45. Yan Y, Wang XJ, Li SQ, Yang SH, Lv ZC, Wang LT, He YY, Jiang X, Wang Y, Jing ZC. Elevated levels of plasma transforming growth factor-β1 in idiopathic and heritable pulmonary arterial hypertension. *Int J Cardiol* 2016;**222**:368–374.
46. Zhang N, Dong M, Luo Y, Zhao F, Li Y. Danshensu prevents hypoxic pulmonary hypertension in rats by inhibiting the proliferation of pulmonary artery smooth muscle cells via TGF-β-smad3-associated pathway. *Eur J Pharmacol* 2018;**820**:1–7.
47. Tang X, Li G, Su F, Cai Y, Shi L, Meng Y, Liu Z, Sun J, Wang M, Qian M, Wang Z, Xu X, Cheng YX, Zhu WG, Liu B. HDAC8 cooperates with SMAD3/4 complex to suppress SIRT7 and promote cell survival and migration. *Nucl Acids Res* 2020;**48**:2912–2923.
48. Ramadhiani R, Ikeda K, Miyagawa K, Ryanto GRT, Tamada N, Suzuki Y, Kirita Y, Matoba S, Hirata K-I, Emoto N. Endothelial cell senescence exacerbates pulmonary hypertension by inducing juxtacrine notch signaling in smooth muscle cells. *iScience* 2023;**26**:106662.
49. van der Feen DE, Bossers GPL, Hagdorn QAJ, Moonen J-R, Kurakula K, Szulcek R, Chappell J, Vallania F, Donato M, Kok K, Kohli JS, Petersen AH, van Leusden T, Demaria M, Goumans M-JTH, De Boer RA, Khatri P, Rabinovitch M, Berger RMF, Bartelds B. Cellular senescence impairs the reversibility of pulmonary arterial hypertension. *Sci Transl Med* 2020;**12**: eaaw4974.
50. Born E, Lipskaia L, Breau M, Houssaini A, Beaulieu D, Marcos E, Pierre R, Do Cruzeiro M, Lefevre M, Derumeaux G, Bulavin DV, Delcroix M, Quarck R, Reen V, Gil J, Bernard D, Flaman J-M, Adnot S, Abid S. Eliminating senescent cells can promote pulmonary hypertension development and progression. *Circulation* 2023;**147**:650–666.